AD-A125 389 FIBER OPTIC MULTIMODE DEVELOPMENT STUDY(U) HUGHES RESEARCH LABS MALIBU CA G L TANGONAN ET AL. DEC 82 RADC-TR-82-315 F19628-80-C-0163 1/1

UNCLASSIFIED F/G 20/6 NL

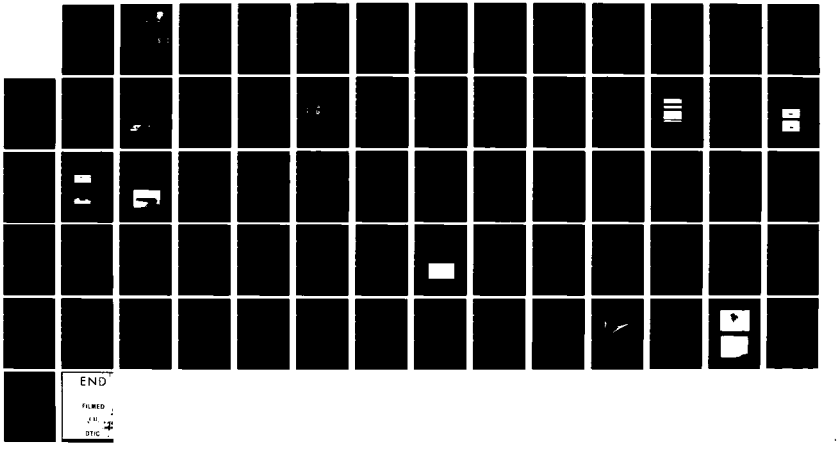

END

FILMED
DTIC

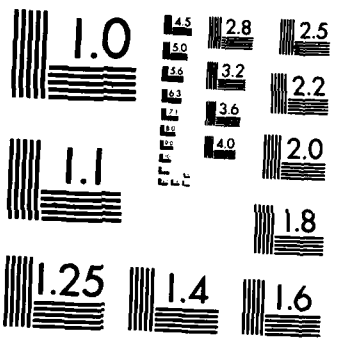

(12)

RADC-TR-82-315
Final Technical Report
December 1982

FIBER OPTIC MULTIMODE DEVELOPMENT STUDY

Hughes Research Laboratories

G. L. Tangonan
H. W. Yen

ROME AIR DEVELOPMENT CENTER
Air Force Systems Command
Griffiss Air Force Base, NY 13441

This report has been reviewed by the RADC Public Affairs Office (PA) and is releasable to the National Technical Information Service (NTIS). At NTIS it will be releasable to the general public, including foreign nations.

RADC-TR-82-315 has been reviewed and is approved for publication.

APPROVED: Richard Payne

RICHARD PAYNE
Project Engineer

APPROVED: Harold Roth

HAROLD ROTH, Director
Solid State Sciences Division

FOR THE COMMANDER: John P. Huss

JOHN P. HUSS
Acting Chief, Plans Office

If your address has changed or if you wish to be removed from the RADC mailing list, or if the addressee is no longer employed by your organization, please notify RADC (ESO) Hanscom AFB MA 01731. This will assist us in maintaining a current mailing list.

Do not return copies of this report unless contractual obligations or notices on a specific document requires that it be returned.

UNCLASSIFIED

SECURITY CLASSIFICATION OF THIS PAGE (When Data Entered)

REPORT DOCUMENTATION PAGE		READ INSTRUCTIONS BEFORE COMPLETING FORM
1. REPORT NUMBER RADC-TR-82-315	2. GOVT ACCESSION NO. AD-A125 389	3. RECIPIENT'S CATALOG NUMBER
4. TITLE (and Subtitle) FIBER OPTIC MULTIMODE DEVELOPMENT STUDY		5. TYPE OF REPORT & PERIOD COVERED Final Technical Report Jul 80 - Jul 81
		6. PERFORMING ORG. REPORT NUMBER N/A
7. AUTHOR(s) G. L. Tangonan H. W. Yen		8. CONTRACT OR GRANT NUMBER(s) F19628-80-C-0163
9. PERFORMING ORGANIZATION NAME AND ADDRESS Hughes Research Laboratories 3011 Malibu Canyon Road Malibu CA 90265		10. PROGRAM ELEMENT, PROJECT, TASK AREA & WORK UNIT NUMBERS 61102E 2306J237
11. CONTROLLING OFFICE NAME AND ADDRESS Rome Air Development Center (ESO) Hanscom AFB MA 01731		12. REPORT DATE December 1982 13. NUMBER OF PAGES 74
14. MONITORING AGENCY NAME & ADDRESS(if different from Controlling Office) Same		15. SECURITY CLASS. (of this report) UNCLASSIFIED 15a. DECLASSIFICATION/DOWNGRADING SCHEDULE N/A

16. DISTRIBUTION STATEMENT (of this Report)

Approved for public release; distribution unlimited.

17. DISTRIBUTION STATEMENT (of the abstract entered in Block 20, if different from Report)

Same

18. SUPPLEMENTARY NOTES

RADC Project Engineer: Dr. Richard Payne (ESO)

19. KEY WORDS (Continue on reverse side if necessary and identify by block number)

Multimode Fiber Optic Couplers
Planar Coupler
Ion Exchange Waveguides

20. ABSTRACT (Continue on reverse side if necessary and identify by block number)

A planar technology has been developed for fabrication of passive couplers for use in multimode fiber optics systems. Based on a previous study (F19628-78-C-0202), the masked ion exchange has been used for guide pattern formation. In this effort an optimization of the diffusion process has been attmepted to maximize the fiber-to-channel coupling.

DD FORM 1 JAN 73 1473 EDITION OF 1 NOV 65 IS OBSOLETE

UNCLASSIFIED

SECURITY CLASSIFICATION OF THIS PAGE (When Data Entered)

The major accomplishments of this program were in the area of processing control and device characteristics and optimization, which resulted in:

- o The achievement of optimization and control of the waveguide formation process; high quality, low loss waveguides can now be fabricated reproducibly.
- o The optimization of fiber-to-channel waveguide coupling through both theoretical and experimental investigations. Meridonal ray excitation <1 dB fiber-to-channel-to-fiber loss has been achieved.
- o A fully packaged fiber-pigtailed 1 x 2 power splitter; the measured total insertion loss is only 2 dB.
- o Fully characterized couplers, particularly with respect to their sensitivity to the input wavelength and the excitation mode group.

These results represent a major advance in the state of the art. We now possess a deeper understanding of the field-assisted diffusion process and are able to translate these insights into improvements in the device performance.

We propose further work to be performed in the following areas:

- o Refinement of masking techniques and diffusion parameters to further improve the index of refraction control.
- o Development of an improved index of refraction profiling technique for mapping the guide profile.
- o Improvements in coupling loss for full model excitation to <1 dB level.
- o Fabrication of advanced devices such as 4- and 8-part star couplers.

TABLE OF CONTENTS

LIST OF ILLUSTRATIONS

SECTION 1

BACKGROUND AND SUMMARY

A. BACKGROUND

Twenty years ago in the spring of 1960, the world's first laser was developed at Hughes Research Laboratories (HRL) in Malibu, California. This pioneering effort, which grew out of a low-noise microwave amplifier program, stimulated widespread interest in the use of light to perform many of the tasks traditionally assigned to microwave systems. The first laser system to be qualified at Hughes to military specifications was a pulsed ruby laser range-finding radar; range finders continue to be one of the primary products of the Hughes Electro-Optic Systems Group. Interestingly, the first fiber-optic device to undergo military qualification testing at Hughes was a delay line for testing and calibrating laser range finders. This simulated optical range test set (SORT) is about the size of a quart-sized can and attaches to a laser range-finder. SORT uses folded optics and the reflection from the end of a long length of special high-strength quartz fiber to simulate targets at ranges up to 1 km. The unique metal-coated, step-index quartz fiber used in SORT was developed at HRL for high-strength (>200 ksi), high temperature (>300°C) applications.

In the early 1970s, the development of long lengths of low-loss optical-fiber transmission lines, operating in conjunction with solid-state optical sources and detectors, promised new solutions to the problems limiting communication and EW systems. In particular, for avionic applications, fiber-guided systems offered:

- Extremely low loss
- Very wide bandwidth
- Immunity from crosstalk, ground loops, electromagnetic interference and interception

- Resistance to radiation damage
- Small size.

Hughes is well aware of the Air Force's needs in communication and electronic warfare systems. During the past several years, we have performed a large IR&D program and several contract studies with the objective of advancing the technological base for designing fiber-optic and integrated-optic (IO) communication and electronic warfare devices and systems.

The Optical Circuits Department of HRL has one of the leading industrial efforts in the world for the research and development of the fiber and optical guided-wave devices and systems for use in specialized avionics applications. This effort currently includes:

- A wavelength-multiplexed fiber-optic data bus for aircraft control systems under a NASA Langley Research Center contract, the key component being the Hughes demultiplexer (see Figure 1).
- A 500-MHz-bandwidth integrated-optical spectrum analyzer with 100 parallel frequency bins for electronic warfare.
- Optical logic devices for ultra-high-speed data processing under AFAL and NSA contracts.
- Passive couplers for multimode and single-mode fibers using ion exchange techniques.
- Radiation-hardened fiber optic research under an ARO contract
- Optical switches and traveling wave modulators for electronic warfare and optic sensor applications.

B. SUMMARY

In this final report we present the results of a research program (F19628-78-C-0207) directed toward the development of fiber optic couplers. This research program will contribute significantly to coupler development for multi-terminal links, a very important problem facing the implementation of fiber optics.

HRL pioneered the use of ion exchange for multimode waveguide couplers.[1] The present program extends the results of a previous Air Force program directed toward coupler development.

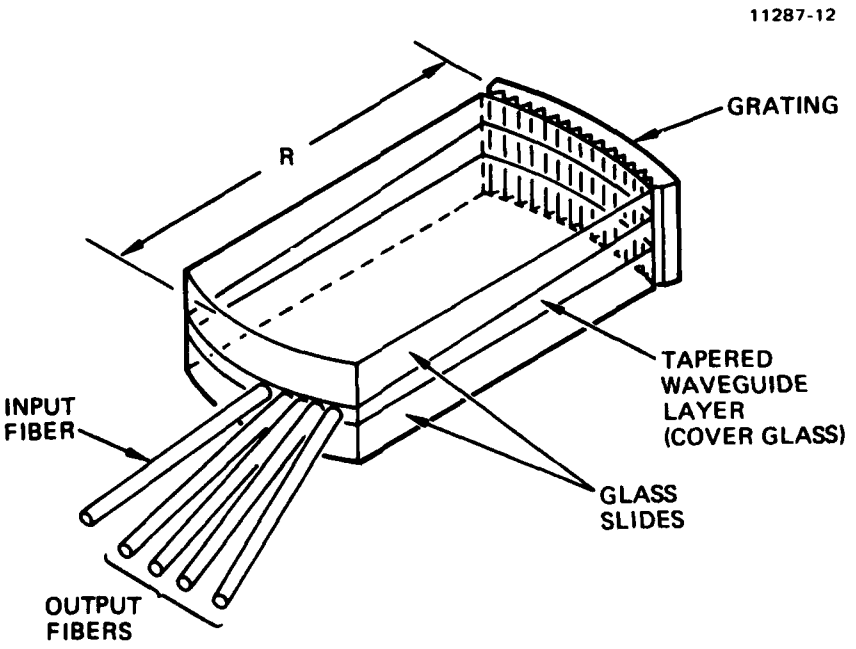

Figure 1. Demultiplexer using a planar guide in a Rowland spectrometer configuration.

In the previous contract (F19628-78-C-0201), which was exploratory in nature, several major accomplishments were demonstrated:

- Design criteria using ray-tracing analysis for coupler fabrication
- Eight-port star couplers and Y-coupler arrays formed by planar processing
- Field-assisted ion exchange for low loss guides (α = 0.3 dB/cm)
- Buried channel guides in borosilicate glass by double exchange
- Buried couplers with 10-dB to 3-dB splitting ratios.

These results represented state-of-the-art accomplishments obtained during the program. In total, they indicate that planar couplers are a feasible alternative to conventional coupler approaches.

In this program (F19628-80-C-0163) we emphasized the following:

- The development of techniques for the fabrication of multimode light-guiding structures on planar substrates. The concern was to obtain a step index and high NA profiles by field-assisted Ag ion exchange.
- The development of pattern definition techniques and waveguide fabrication using photolithographic approaches.
- The design and fabrication of planar access couplers, power splitters, and star couplers suitable for coupling with standard commercial step and graded-index fibers. Primary consideration was throughput optimization.
- The evaluation of the fabricated devices with LED and laser excitation in the 0.8-1.3 μm range.

The major accomplishments of this program were in the area of processing control and device characterization and optimization, which resulted in:

- The achievement of optimization and control of the waveguide formation process; high quality, low loss waveguides can now be fabricated reproducibly.
- The optimization of fiber-to-channel waveguide coupling through both theoretical and experimental investigations. Meridonal ray excitation <1 dB fiber-to-channel-to-fiber loss has been achieved.
- A fully packaged fiber-pigtiled 1 x 2 power splitter; the measured total insertion loss is only 2 dB.
- Fully characterized couplers, particularly with respect to their sensitivity to the input wavelength and the excitation mode group.

SECTION 2

TECHNICAL SUMMARY

A. INTRODUCTION

1. Current Approach to Coupler Fabrication

Multimode fiber-optic systems currently use couplers for data distribution to several user terminals. Couplers are made by modifying the optical fibers (fusing, tapering, lapping, and gluing), or with micro-optic components (such as microlenses and beam splitters). These two approaches and the planar approach, which is the subject of this proposal, are shown in Figure 2. Good couplers have been demonstrated using micro-optic methods, although several key questions have been encountered when attempting to transfer the technology to a manufacturing process.

The cost of mass produced couplers is greatly affected by the reproducibility of the fabrication technique. In the fused fiber approach, the problem of reproducibility is most severe. Controlling the electric discharge (or flame torch) conditions and the mechanical devices for tapering the fused region of the fibers continues to require considerable development. Hughes is actively pursuing techniques to solve these problems to enable us to manufacture the fused coupler. This work is being pursued by the Hughes Connecting Devices Division at Irvine, California.

Component placement and packaging in current micro-optic devices requires considerable attention during coupler assembly. Each element must be anti-reflection (AR) coated to minimize reflection losses and maintain high isolation. The cost of the individual components — SELFOC lenses, beam splitters, and precision machined placement devices — may prove to be quite prohibitive.

The proposed planar fabriction approach (shown in Figure 2) directly attacks the problems of reproducibility, one-by-one fabrication, and precise placement of components which are encountered in the two conventional approaches by emphasizing the photolithographic control of the coupling structure and the batch processing capabilities inherent in planar processing. A schematic of the fabrication process is shown in Figure 3. The basic processing steps illustrated are mask deposition, photo-etching for pattern definition, and ion exchange processing. These are techniques that are well developed for

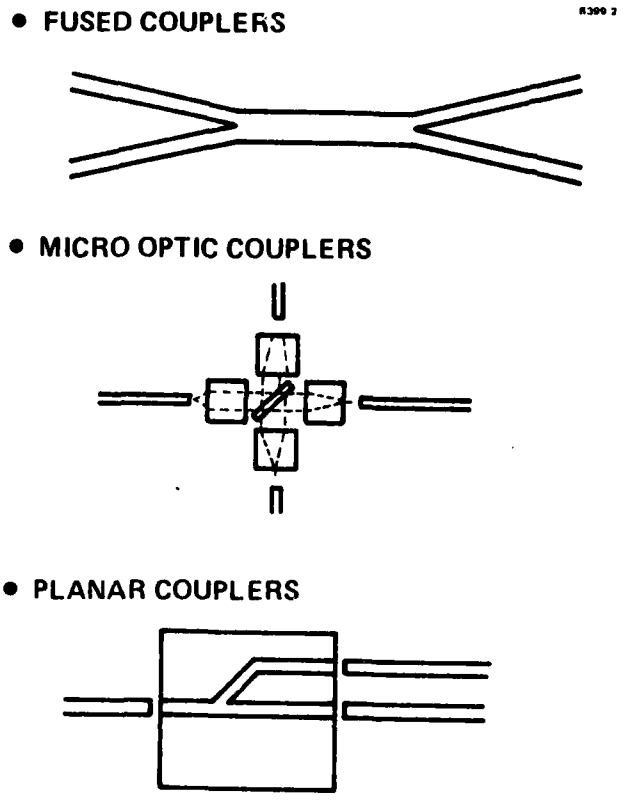

Figure 2.
Schematic of the three approaches to coupler fabrication.

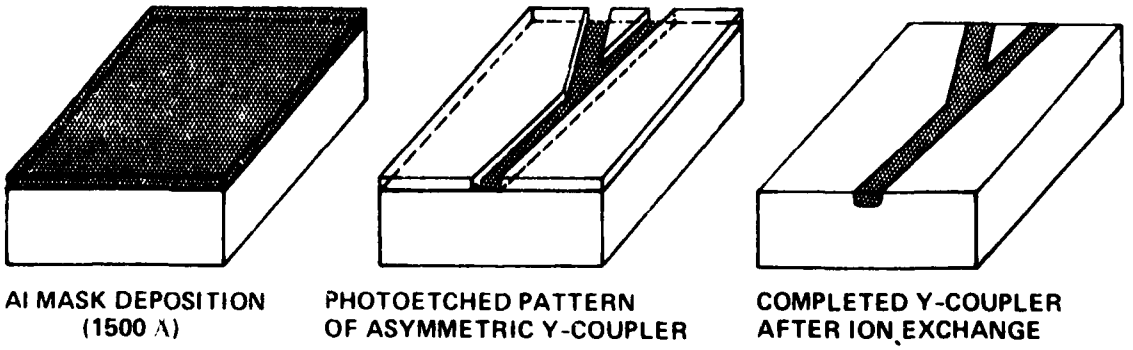

Figure 3. Masked ion exchange process for coupler fabrication.

processing microelectronics; the benefits of reproducibility, batch processing, and low cost are obvious. In addition, the positioning of components is largely eliminated by the pattern definition and use of precision V-groove holders for interfacing the fibers. All of these steps have been fully demonstrated in the previous coupler programs.

The technical program was based on our recognition of the essential elements required for the optimization of planar couplers. The key elements of our approach (dicussed individually below) were:

- Guide formation process control
- Throughput optimization (fiber-to-channel-to-fiber)
- Coupler fabrication and fiber interfacing.

Each of these elements have undergone considerable investigation under this program.

B. GUIDE FORMATION PROCESS CONTROL

1. Guide Formation Processes

Waveguide formation in glass can be accomplished by several techniques. These techniques include chemical vapor deposition, ion exchange and diffusion, dip coating, ion implantation, and laser heating. Three years ago, HRL researchers began investigating these various processes for fabricating multimode guides. To date, the preferable approach is clearly ion exchange. In this proposal, we emphasize field-assisted ion exchange as the preferred approach.

In the past, various ion exchange and diffusion systems have been studied. The approaches we have tried at HRL include:

(1) Li_2So_2-K_2SO_4 eutectic salt melt/soda lime glass

(2) LiCl-KCl eutectic salt melt/soda lime glass

(3) Ag metal field-assisted diffusion (solid phase)/soda lime glass

(4) $AgNO_3$ melt/soda lime glass (with and without fields)

(5) $AgNO_3$ melt/borosilicate glass (with and without fields)

(6) Double exchange $NaNO_3$ and $AgNO_3$ borosilicate glass.

The most successful ion exchange systems have been (1), (5), and (6). Our description of guide formation provides the details of these three processes.

The formation of optical waveguides in planar substrates has been the subject of intensive research in the area of integrated optics. The thrust of these studies has, however, been directed toward single-mode device applications. More recently, multimode fiber optic devices have been made that are quite promising. Auracher et al[2] reported the first planar branching networks formed in photo-polymer material of 100-μm thickness. Wilson et al[3] described the use of Ag/Na exchange for guide formation and simple coupler designs. Researchers at Hughes have described the utilization of ion exchange processes in glass to fabricate couplers, star couplers,[4] and even wavelength demultiplexers.[5]

The ion exchange process utilized by the Hughes team in these previous works was that developed by Chartier et al.[6] In this process, a eutectic mixture of Li_2SO_4 and K_2SO_4 is heated under an oxygen atmosphere to 580°C. A sodium glass slide is suspended over the melt for 30 min to reach thermal equilibrium with the melt. Next, it is dipped into the melt for 20 min, and then is again suspended over the melt for 10 min to avoid any thermal shock. The process is illustrated in Figure 4, along with the phase diagram for Li_2SO_4-K_2SO_4. Planar waveguides, 100 μm deep, are made by this process. The coupler structures are formed by masking with a thick (1 to 2 μm) Al film. The Al mask is subsequently removed by dipping the slide in hot 6 HCl solution. This process provides an index difference (NA ≈ 0.1) that is too small to cope with larger numerical aperture fibers (NA > 0.2). However, despite this drawback, this process has been quite successful in demonstrating planar processing of coupler devices.

2. Fabrication of Waveguides by Field-Assisted Ion Exchange

To circumvent the problem of low index of refraction change, an alternative diffusion process was developed: Ag ion exchange under a field. This process is similar to that described by Chartier et al,[7] and Izawa and NaKagome.[8] When the ion exchange is carried out in the presence of an electric field, the concentration profiles (and thereby the index of refraction) are considerably modified. The concentration of the ions during the process is given by:

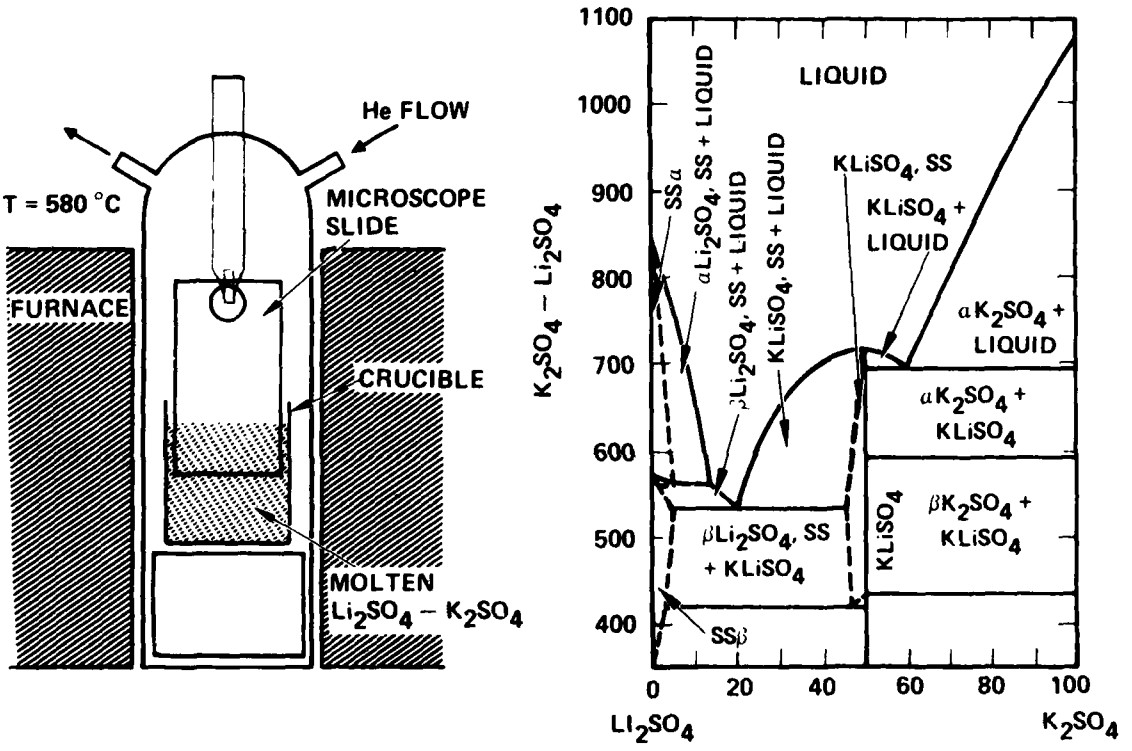

Figure 4. Guide formation processes using Li_2SO_4-K_2SO_4 eutectic melt.

$$\frac{dC}{dt} = D \frac{d^2C}{dZ^2} - E\mu \frac{dC}{dZ} \quad , \tag{1}$$

where the variables C and t are the concentration and diffusion times, respectively, and the diffusion parameters D, E, and μ are the diffusion constant, applied electric field, and the ion mobility, respectively. When the initial concentration of Ag in the glass is zero and an equilibrium surface concentration of C_o is attained, the resultant profile is given by

$$C(Z,t) = C_o \text{ erfc } [(Z - E\mu t)/2\ (Dt)^{1/2}] \quad , \qquad (2)$$

which, for E = 0, reduces to the result for normal diffusions without a field.

Figure 5 shows the concentration profiles attainable by electric field and normal exchange processes. The implication of the profile differences are:

- The field-assisted profile is predominantly a step-index with a graded junction into the substrate.
- The product, Eμt, essentially controls the depth of the planar step-index guide.

The experimental apparatus used to demonstrate electric-field-assisted diffusion is shown in Figure 6. A double-crucible arrangement was used to provide a molten salt bath on both sides of the sample. This eliminated Na buidup at the negative electrode side of the substrate. Depending on the polarity of

9748-3

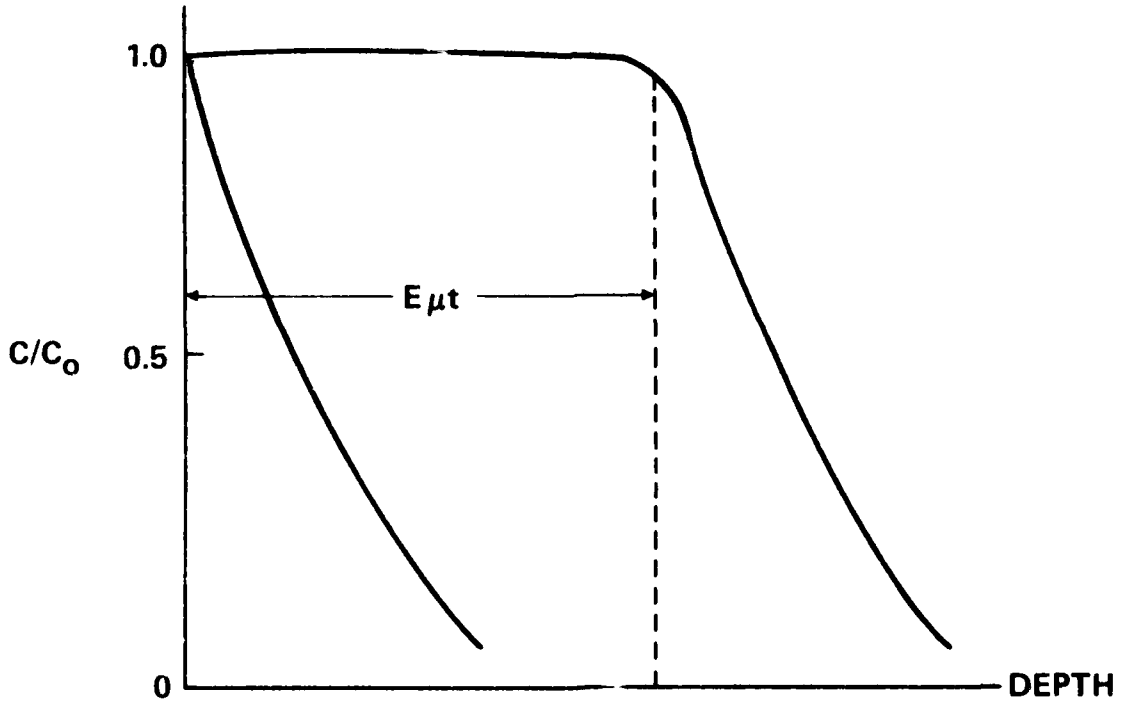

Figure 5. Diffused profile obtained with field-assisted diffusion.

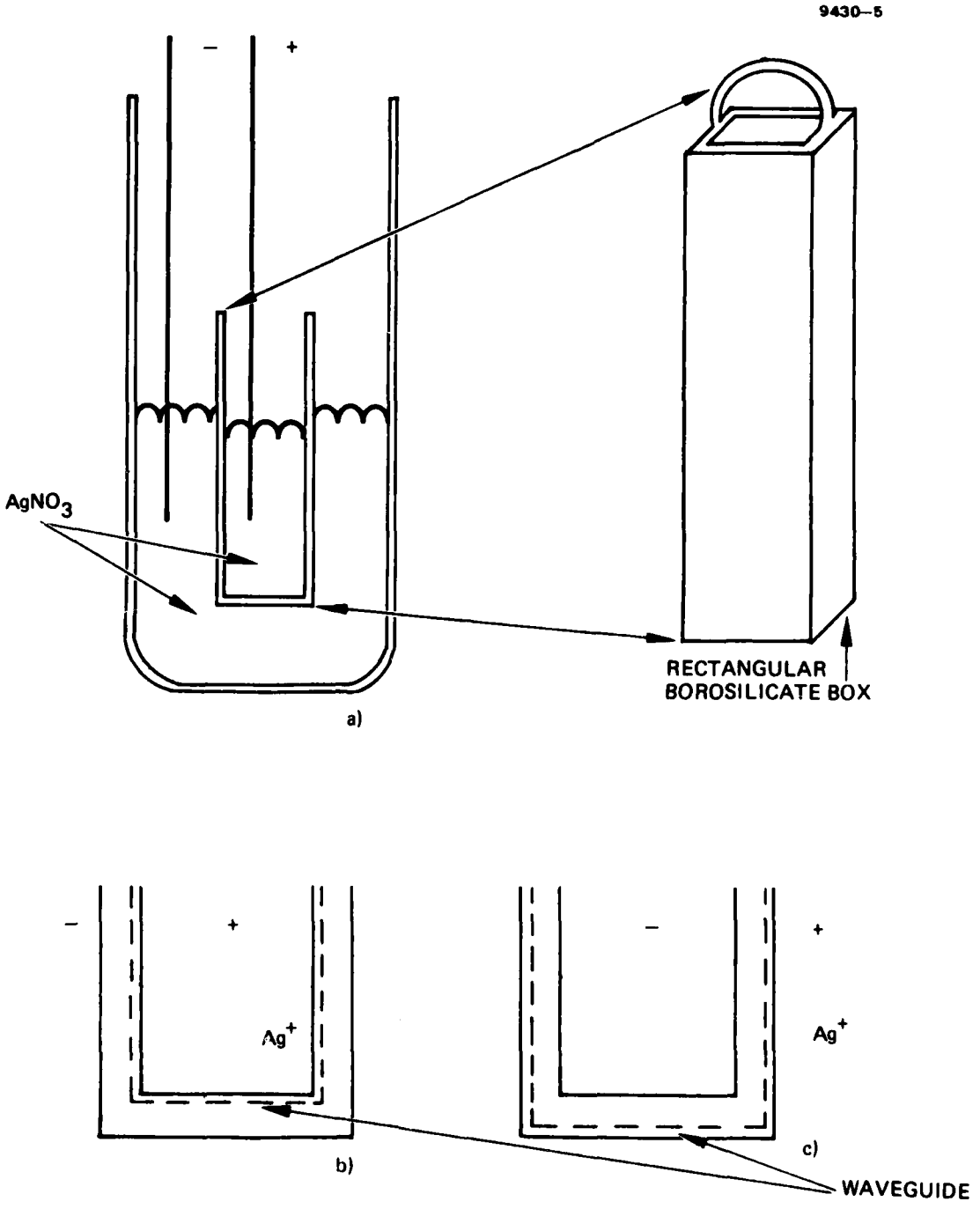

Figure 6. Double crucible apparatus for guide formation; depending on the polarity of the electrodes (a) guide formation occurs on inner (b) or outer (c) surface.

the electrodes, the ion exchange occurs on either side of the sample. Borosilicate glass was used because we found that it is readily shaped into the double crucible configuration, shows little sample warping, and is free from the Ag migration problems observed in soda lime glasses. The parameters used for planar guide formation are given in Figure 7. Deep planar waveguides of low loss are obtained using these parameters. From these results an approximate measure of the ion mobility of Ag at 370°C in the glass is given by

$$\mu = 10 \times 10^{-10} \frac{cm^2}{sec\ V} \quad . \tag{3}$$

The index profile obtained for the waveguides was measured using standard interferometric techniques. The result obtained for one of the samples (E) is shown in Figure 8.

9430-7

SAMPLE	T, °C	t, HRS	E, V/mm	I, mA	WAVEGUIDE DEPTH, μm
A	370°C	4.5	33	–	52
B	370°C	1.0	100	–	55
C	370°C	2.5	50 – 230	10	25
D	370°C	3.0	50	–	70
E	300°C	4.2	150	–	35

Figure 7. Waveguide depth for Ag ion exchange versus temperature, time, and field.

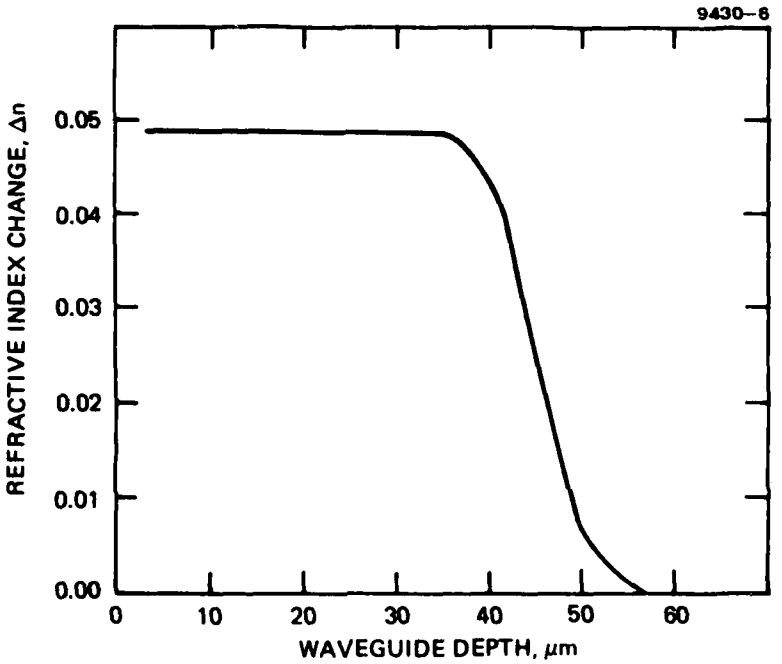

Figure 8. Index of refraction profile for sample E. Note the step-like index profile measured by interferometric methods.

3. Buried Planar Waveguide Formation

Buried waveguides have been formed by a second field-assisted exchange process using $NaNO_3$. In this process, Na is reintroduced in the surface refraction at the surface is shown in Figure 9. Waveguiding experiments show that the additional confinement layer at the surface shows a dramatic difference in optical waveguide output profile. This output of two guides, with and without burying, is shown in Figure 10.

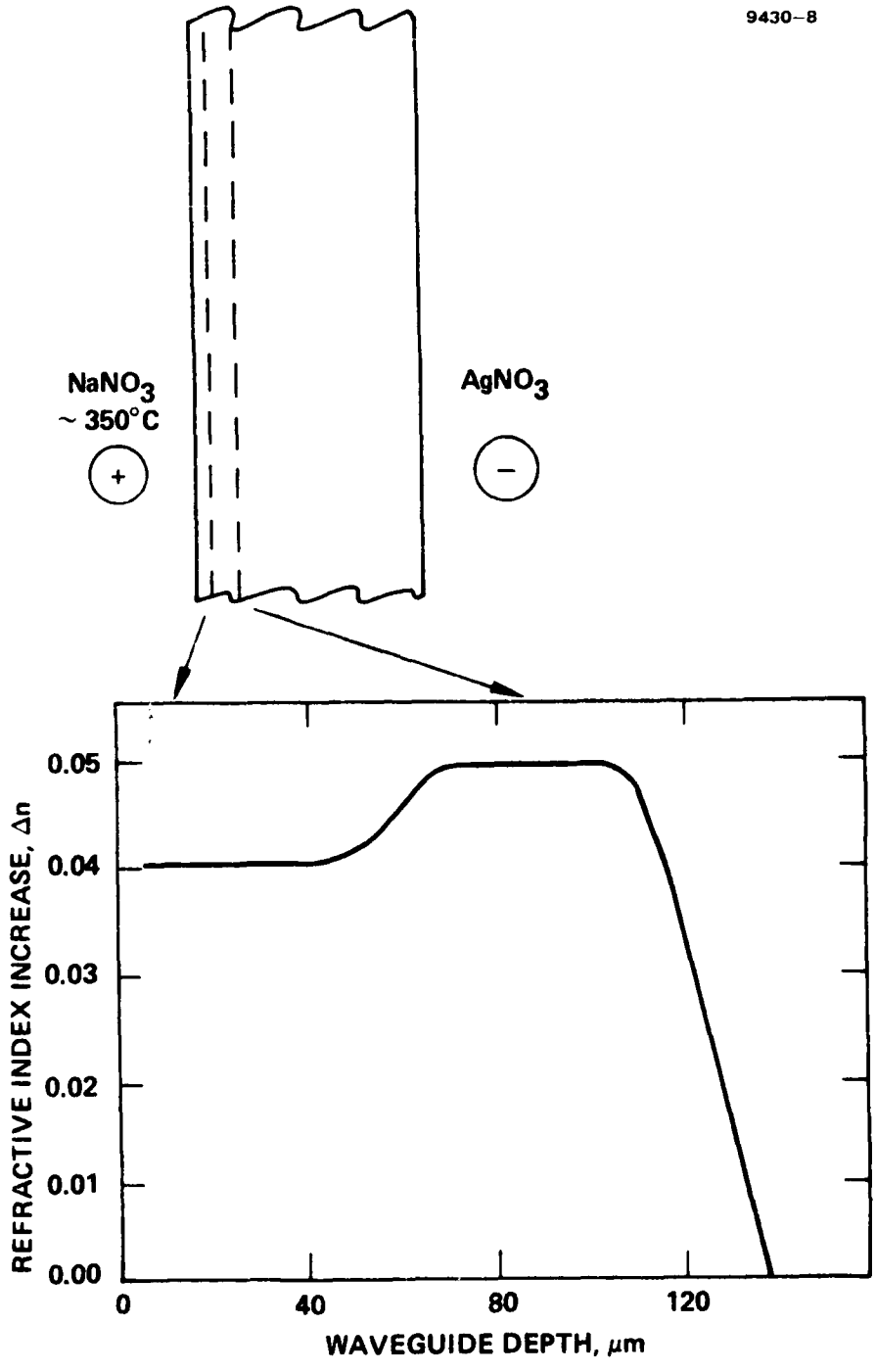

Figure 9. Double exchange formation of buried waveguides. The burying is incomplete, although the index drop of 0.01 is still substantial.

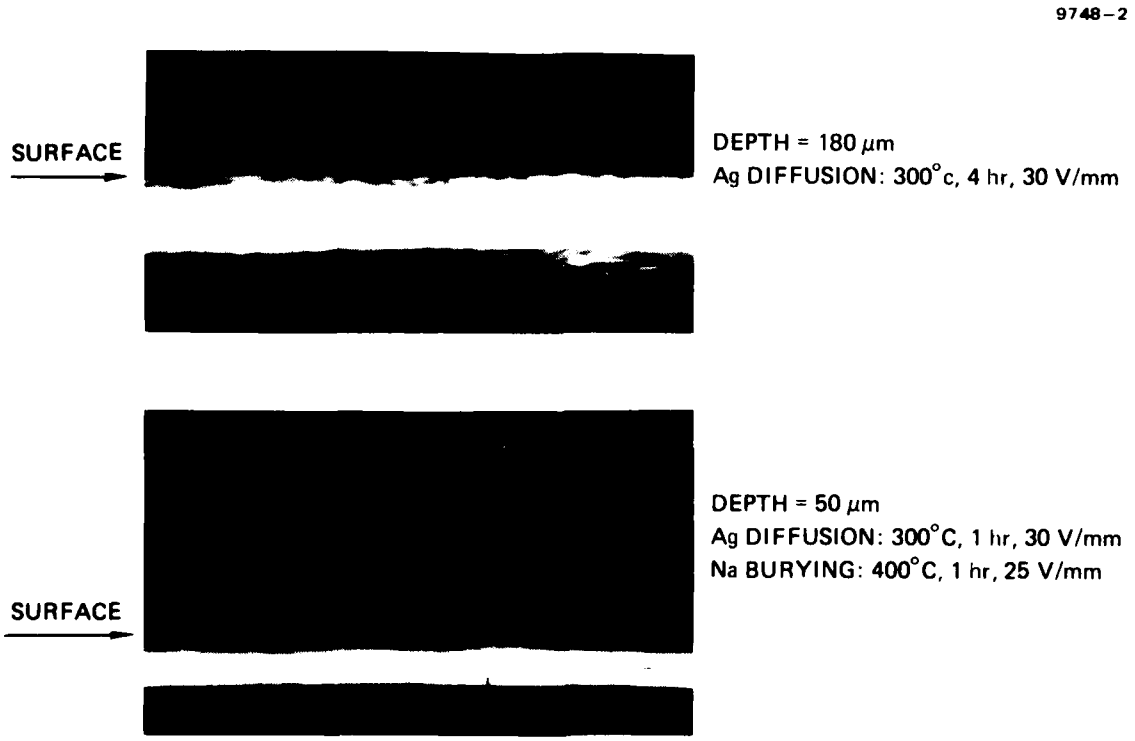

Figure 10. Buried planar waveguides compared to unburied guides. Processing: Ag diffusion 300°C, 1 hr, 30 V/mm and Na diffusion 400°C, 1 hr, 25 V/mm.

4. Buried Channel Waveguide Fromation

Channel waveguides can be formed by using an aluminum mask for blocking the exchange process. Channel waveguides formed in this way can be buried using the same process described above.[9] A comparison of the output profiles for two waveguides formed with and without burying is shown in Figure 11. A clear difference is observed between the two waveguide output profiles. In the laboratory, the buried waveguides show a remarkable uniformity along the length of the guides when excited by light. This is in contrast to the case of the unburied guides in which surface scattering due to cracks in polishing scratches is seen as bright scattering sites.

5. Applications Potential of Planar Couplers

Based on previous results,[3,4] the major problem area in exploiting the planar coupler is to reduce the coupling losses encountered in mating input and output fibers with the coupling structure. In recent experiments on Ag ion exchange samples, major improvements in the throughput from fiber to channel to fiber has been demonstrated. For unburied guides, the throughput loss is as low as 1.1 dB. For buried guides, losses of <1 dB have been measured. This result makes planar coupler structures quite competitive with conventional fusion approaches. That a variety of structures can be made by photolithographic control of the diffusion masks has already been established by our previous results.[3,4]

6. Problem Areas and Optimization

We encountered several problems in the area of material processing during the technical program. The problems were:

- Incomplete burying of the waveguides with current techniques;
- Edge effects during masked ion exchange which cause the thickness variations of the waveguides;
- Optimization of buried channel guides for high throughput efficiency; and
- Refractive index profile measurements using the refractive near field technique.

The first two of these problem areas require elaboration. Incomplete burying of the waveguides is deleterious if the effective index barrier for the buried interface is too low. Presently, the surface index difference is 0.01. This should be increased to at leat 0.015 so that optical fibers with numerical apertures of >0.20 can be accommodated. Our investigations will concentrate on varying the diffusion conditions to increase the confinement.

In a recent publication, Aksenov et al[10] have summarized the attainable index differences for various melts. When very high Δn's are required, $\Delta n <$ 0.08 of the melt combination of KNO_3:$AgNO_3$ melts are superior to KNO_3:$AgNO_3$ and $NaNO_3$:$AgNO_3$. They have shown that the maximum change in the refractive index at the waveguide surface, $\Delta n(o)$, is related to the mode concentrations of the nitrates in the mixtures, z_1 and z_2, by

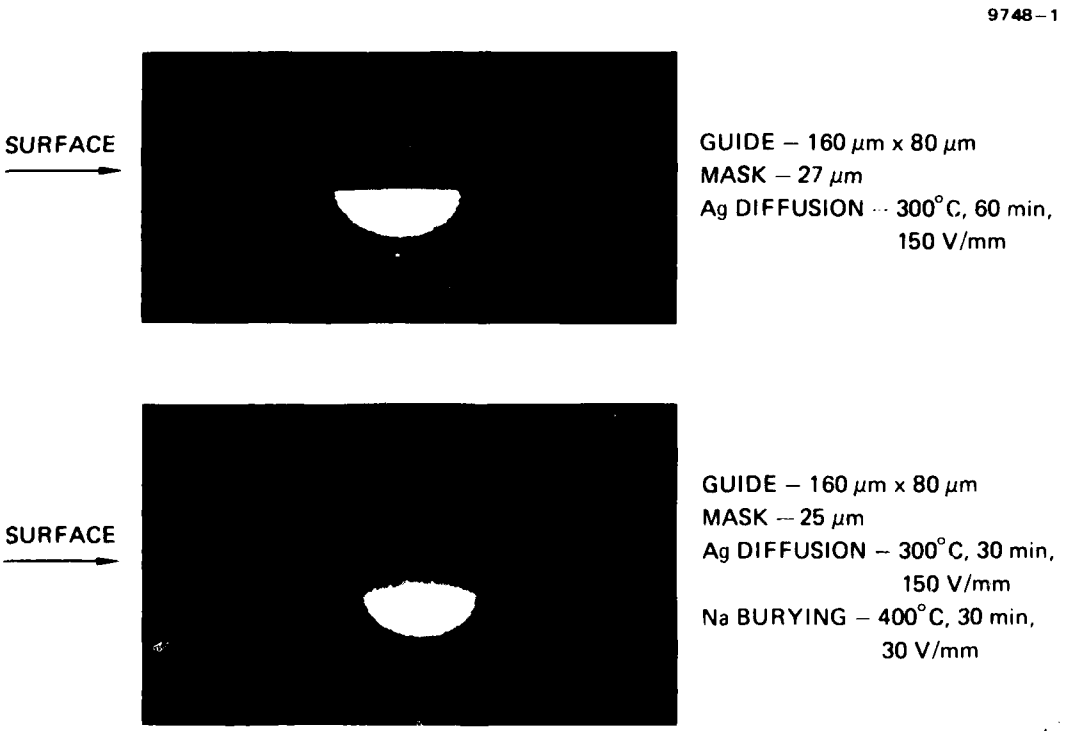

Figure 11.
Buried channel waveguides (160 μm x 80 μm) compared to unburied gates. Processing: 25 μm mask width. Ag diffusion -300°C, 30 min, 150 V/mm, Na burying -400°C, 30 min, 30 V/mm.

$$\ell n \frac{z_1}{z_2} = \frac{B_{12}}{RT} \frac{z_1 - z_2}{M} = \gamma \ln \left[\frac{\Delta n(o) - \Delta n_2(o)}{\Delta n_1(o) - \Delta n(o)} \right] + \text{constant} \quad , \qquad (4)$$

where R is the universal gas constant, B_{12} is the mutual exchange energy, m is the molar mass of the melt, and $\Delta n_1(o)$ and $\Delta n_2(o)$ are the index changes at the surface due to single nitrate diffusions.

The numerical apertures of the guide layers can be lowered by using one melt ($NaNO_3$-$AgNO_3$) for the first processing, as opposed to pure $AgNO_3$, then a different set of mixtures must be used to obtain more complete burying. At present, a pure $NaNO_3$ melt is preferred to the burying with a composition of <3.9% $AgNO_3$ (in $NaNO_3$) for a $\Delta n = 0.025$ (NA = 0.27), this Δn being one-half our present value. This procedure was not attempted on this program; it is a major new insight which is applicable for further work.

The second problem area, edge effects caused by a diffusion through a mask, is illustrated in Figure 12. For the same diffusion conditions, the effective diffusion depth varies depending on the position relative to the mask. This effect depends on the mask width as well. The results shown are, in fact, for the same sample. The planar guides (no mask) are remarkably thinner than for guides formed through a mask. The contrast in results for wide and narrow masks is also quite interesting. For the wide mask (500 μm), the tendency for thinner guide depths is observed at the center of the guide region. Near the mask edges, an enhanced diffusion is observed. For the narrow mask (35 μm), the expected semicircular profile is observed. Chartier et al[11] recently reported similar observations. Their explanation of the observed shape of the profiles is based on an electrochemical bias between the silver nitrate bath and the metallic mask. An electrical field, in their interpretation, is generated by this electrochemical bias.

Current work at HRL differs significantly with Chartier's interpretation. We replaced the metallic mask (Al) with a nonconducting mask (SiO_2) and studied the edge effects. Almost identical results have been measured. However, these results are complicated by the incomplete blocking of the SiO_2 layer. The waveguide profile for the SiO_2 mask is shown in Figure 13. The same diffusion conditions were used to closely compare to the results obtained with the metallic mask. Detailed measurement of the guide shape shows very close similarities.

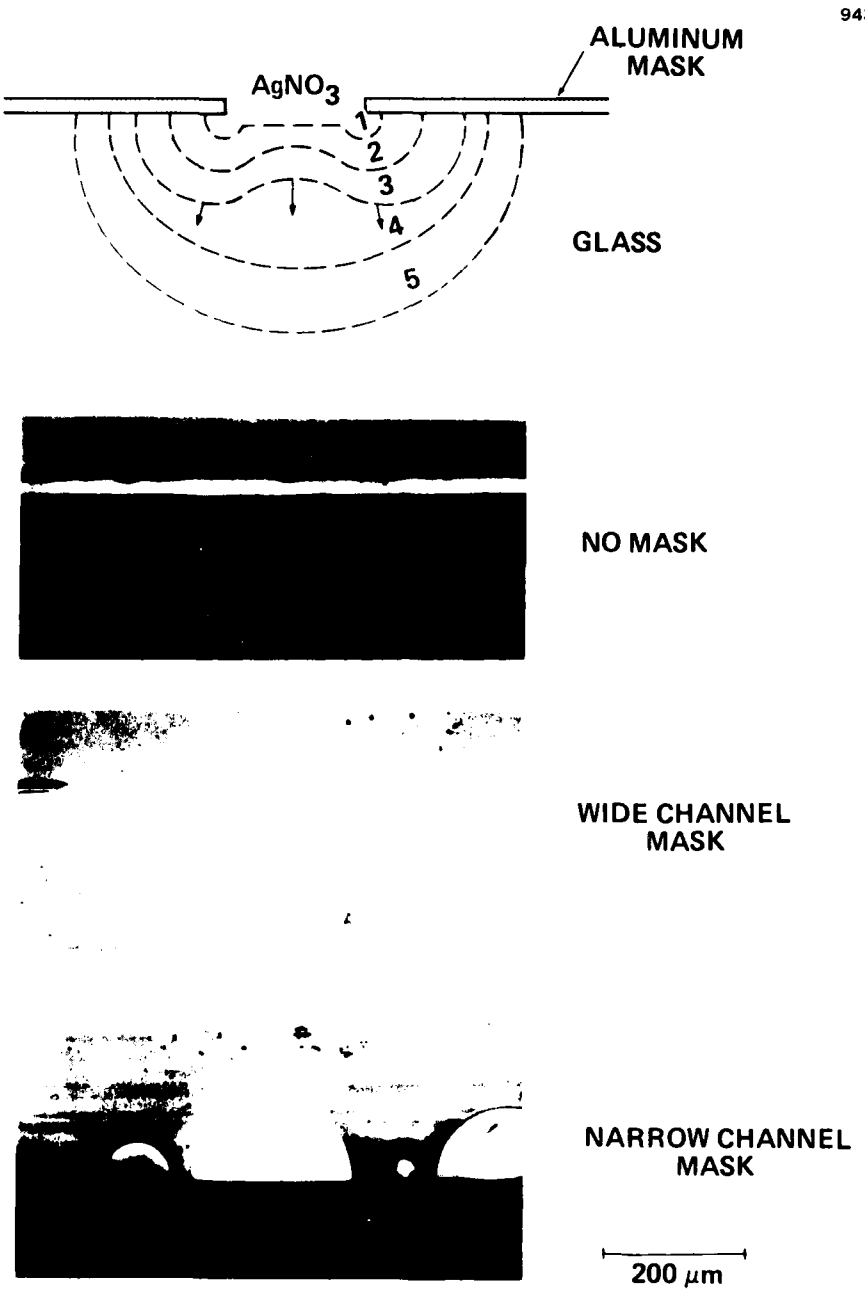

Figure 12. Effects caused by enhanced diffusion at the mask edge (Al). Note the variation in guide depth with mask width.

When viewed in the light of the experiments, the interpretation of Chartier et al is in error, since the same effects are observed for what should clearly be different electro-chemical systems. As described in the next section, the effect is now understood to be caused by the field distribution under the mask. By varying the applied field, the extent of the thinning is controllable. Detailed measurements of this effect should be pursued using improved index profiling.

The technical significance of this problem cannot be minimized. The fabrication of star couplers, which requires very wide masks (several mm's) to form the mixing region, is complicated by the guide thinning effects. The high index guides we have used are overmoded when compared to the excitation conditions using conventional fibers (NA $\cong$ 0.2). Guide thinning effects may not severely affect star performance, but a closer examination is necessary. In fact, we consider the effect of the guide thinning to be the critical materials processing limit to the design flexibility.

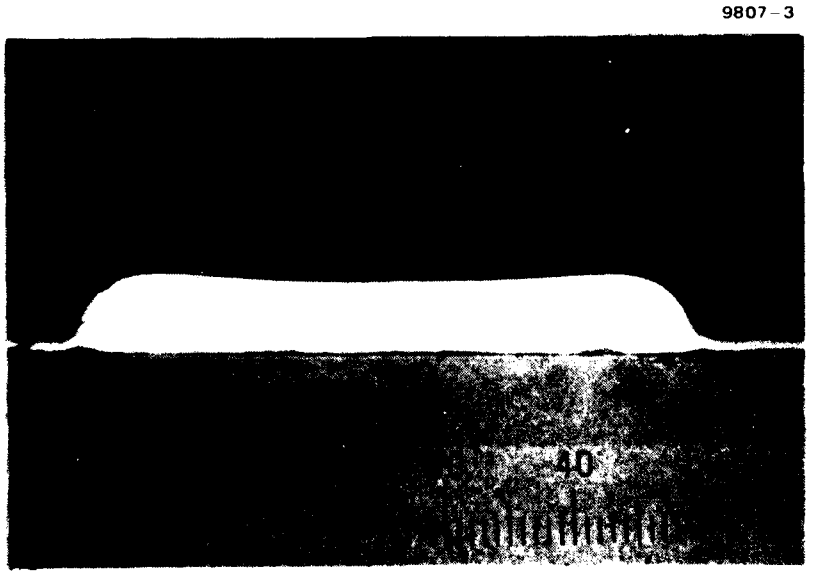

t = 30 min
E = 166 V/M
W = 500 μm

Figure 13. SiO_2 mask results.

7. Diffusion Equation for Field-Assisted Exchange

During our research program a detailed understanding has been attained for waveguide shape resulting from field-assisted ion exchange. In reviewing the mathematics of the diffusion process in detail, we can show how the problems of thinning of the waveguide for wide masks and the lobe formation under the mask are a consequence of the field distribution for the different mask configurations. This result was first discussed by Voges,[12] who extended the work of Copper and Abou el Leil[13] to channel guides.

For the case of an Ag-Na ion exchange, one configuration is shown in Figure 14 which utilizes two melts on either side of the sample. In this way Na_+ accumulation at the negative electrode is avoided. For the sake of the mathematical description the situations are equivalent.

The ionic flux for the two mobile species, j_{Ag} and j_{Na}, must be a constant function throughout the sample for the case of planar guide formation (no mask). The concentrations (molar), C_{Ag} and C_{Na}, are therefore such that $C_A + C_B = Co$, where Co is the total alkali concentration. The various quantities, j_{Ag}, j_{Na}, the applied field, E, and the concentration distribution are related by

$$j = -D \frac{\partial C}{\partial X} + E\, C_A D_A / KT \quad . \tag{5}$$

The concentration of Ag is determined by solving the diffusion equations.

$$\frac{\partial C}{\partial t} = \frac{1}{[C_o + (M-1)C]}\, 2 \left(\{C_o [C_o + (M-1)C] D\} \frac{\gamma^2 C}{\gamma X^2} \right.$$

$$- \left\{ C_o + (C_o - C)C \frac{\gamma \ell n M}{\gamma C} \right\} MJ \frac{\gamma C}{\gamma X}$$

$$\left. - \left\{ (M-1) + CM \frac{\gamma \ell n M}{\gamma C} - [C_o + (M-1)C] \cdot \frac{\gamma \ell n D}{\gamma C} \right\} DC_o \left(\frac{\gamma C}{\gamma X} \right)^2 \right) \quad . \tag{6}$$

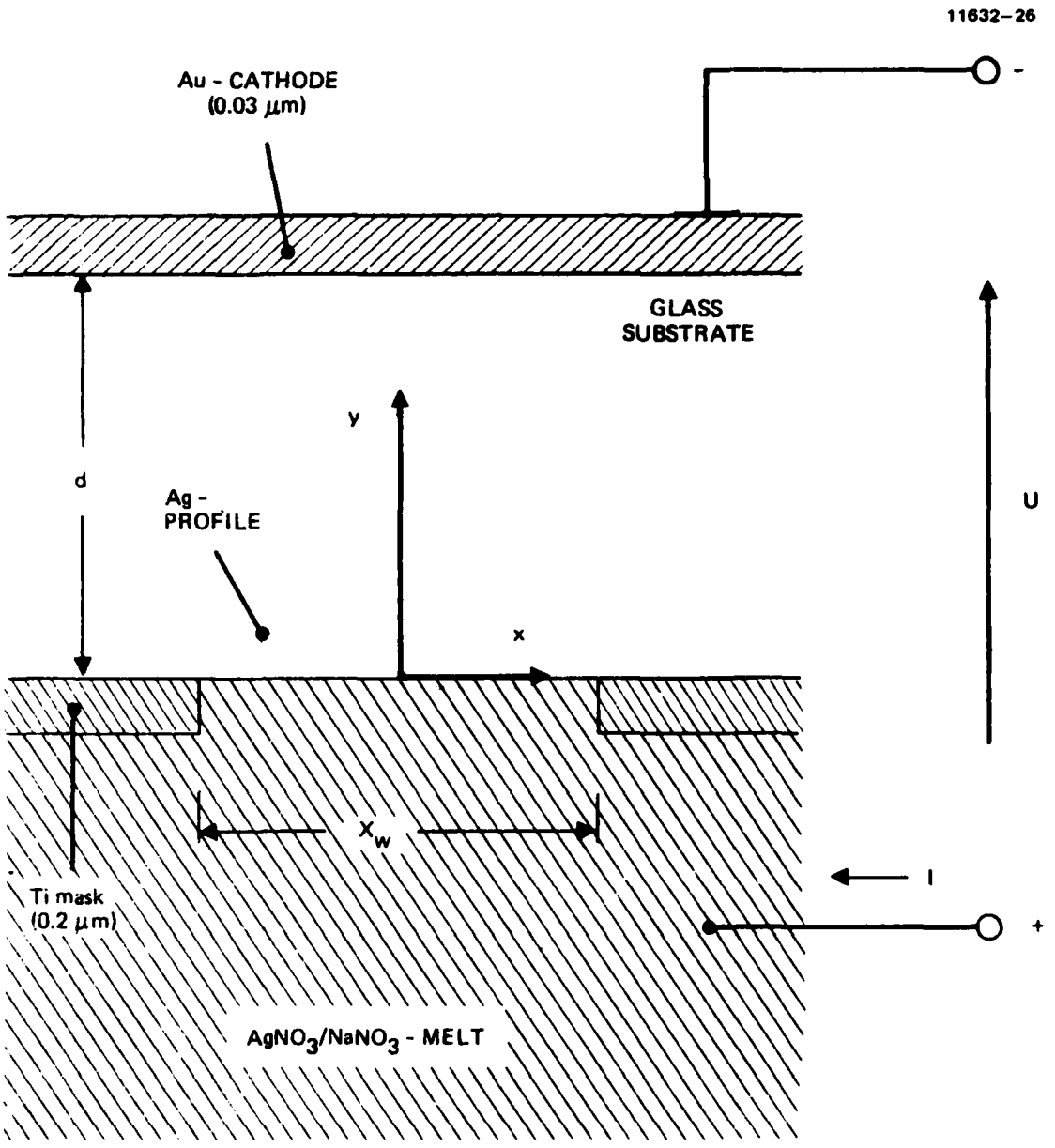

Figure 14. Configuration of a field-assisted ion exchange in glasses.

where $C = C_{Ag}$, $D = D_{Ag}$, $J = j_{Ag} + j_{Na}$. This is the complete diffusion equation, including concentration-dependent diffusion. The diffusion coefficients are concentration-dependent for alkali ions in silica glasses; this is called the mixed ion effect.[14] For this discussion, however, we ignore these effects. In this case the equations simplify to the following form:

$$\frac{\gamma C}{\gamma t} = \frac{C_o D \left[\frac{\gamma^2 C}{\gamma X^2}\right]}{C_o + (M-1)C} - \frac{C_o M J \left(\frac{\gamma C}{\gamma X}\right)}{\left[C_o + (M-1)C\right]} - \frac{(M-1)DC_o \left(\frac{\gamma^2 C}{\gamma X}\right)^2}{\left[C_o + (M-1)C^2\right]} \quad . \tag{7}$$

Furthermore, when the flux density, j, is very high, the terms in $\gamma^2 C/\gamma X^2$ and $\gamma C/\gamma X$, which depend on D, may be neglected, so that the diffusion under field conditions can be written[15] as

$$\frac{\gamma C}{\gamma t} = \frac{-MjC_o}{\left[C_o + (M-1)C_o\right]} \cdot \frac{\gamma C}{\gamma X} \quad . \tag{8}$$

One interesting result, obtained by Abou el-Leil,[16] is that for the case of constant total concentration of alkali ions in the glass, $dC/dt = 0$. Therefore,

$$\frac{\gamma C}{\gamma t} + \left(\frac{\gamma X}{\gamma t}\right)_c \left(\frac{\gamma C}{\gamma X}\right)_t = 0 \quad , \tag{9}$$

or

$$\left(\frac{\gamma X}{\gamma t}\right)_c = \frac{MjC_o}{\left[C_o + (M-1)C\right]^2} \quad . \tag{10}$$

Thus, for modifying a given index profile by imposing a net flux, j, the position of constant concentration, X, moved with the velocity $(\gamma X/\gamma t)_C$. Since the total current density is proportional to ΔV, the potential difference, the displacement by ΔX of the profile shape, can be attained by varying either parameter ΔV or t. This is true, of course, as long as ΔV is sufficiently large so that our derived equations remain valid.

In the more typical case, Ag ions are introduced into the glass from a molten salt under electric field conditions. Let us call the concentration of Ag in the glass in equilibrium with the melt, Ce, and Cg the concentration of Ag in the glass initially. For our consideration, $C_e > C_g$; a step function discontinuity occurs at the melt/glass interface. For the case of Ag exchanged into Na based-glasses, the higher mobility of the Na atoms would lead to separation of charge species (Ag_+ and Na_+). However, the space charge field formation couples the Na^+ migration to the slower moving Ag^+ ions. For the case of $D_{Ag}/D_{Na} < 1$, an asymptotic solution exists:

$$\frac{C - C_g}{C_e - C_g} = \left\{1 + \exp\left[\frac{V(1 - M)(C_e - C_g)(X - Vt)}{DC_o}\right]\right\}^{-1} , \qquad (11)$$

where

$$V = \frac{MjC_o}{[C_o + M - 1)\ C_g][C_o + (M - 1)\ C_e]} . \qquad (12)$$

For in the case in which the concentration of Ag in equilibrium with the melt Ce is equal to the total concentration of alkali ions, C_o, and $C_g = 0$,

$$\frac{C}{C_o} = \left\{1 + \exp\left[\frac{1}{C_o D}(1 - M)\left(X - \frac{1}{C_o} t\right)\right]\right\}^{-1} \qquad (13)$$

and

$$V = \frac{j}{C_o} \quad . \tag{14}$$

As stated before, the asymptotic distributions have been presented. The approach time, τ, for the step profile to evolve to the final profile given above is given by $\tau = C_o^2 D/j^2[(1 - M)]^2$. Several workers have shown that this time is far less than the normal times for diffusion.[17]

Voges has pointed out[12] that a simple step solution applies rather well for deep guides. He compared the solution given above and the solution of Chartier[18] which neglects the space charge effects with a simple step from the step wall moving with velocity, V. His comparison is shown in Figure 15.

Using this simplified solution Voges addressed the problem of masked exchange. The configuration he studied is shown in Figure 16. The shape of the uniform index distribution is given by the position vector of the Ag ion front,

$$\vec{r}_f = X_o e_x + \int_o^t \mu_{Ag} \vec{E} dt \text{ for } -\frac{W}{2} \leq X_o \leq \frac{W}{2} \tag{15}$$

for an exchange time, t. The electric field configuration is equal to the static field of the triplate transmission line,

$$E = Ex + iEy = j \frac{\pi}{2} \frac{U}{dK'(K)} \cdot \left| \frac{\tanh^2 u - 1}{\tanh^2 u - K^2}^{1/2} \right| , \tag{16}$$

where $u = \pi (x - jy)/2d$, $K = \tanh \pi (xw/4d)$, and $K'(k)$ is the Jacobian elliptic function. Figure 16(a) and (b) shows the calculated index profiles for several applied voltages, $T = 616°K$, $t = 30$ min, $d = 300$ μm, and $D_{Ag} = 2.6 \times 10^{-15}$ m^2/s. These conclusions are quite similar to our results for the guide shape for different mask widths. Voges has obtained further confirmation by measuring the index profile using Nomarsky interference techniques.

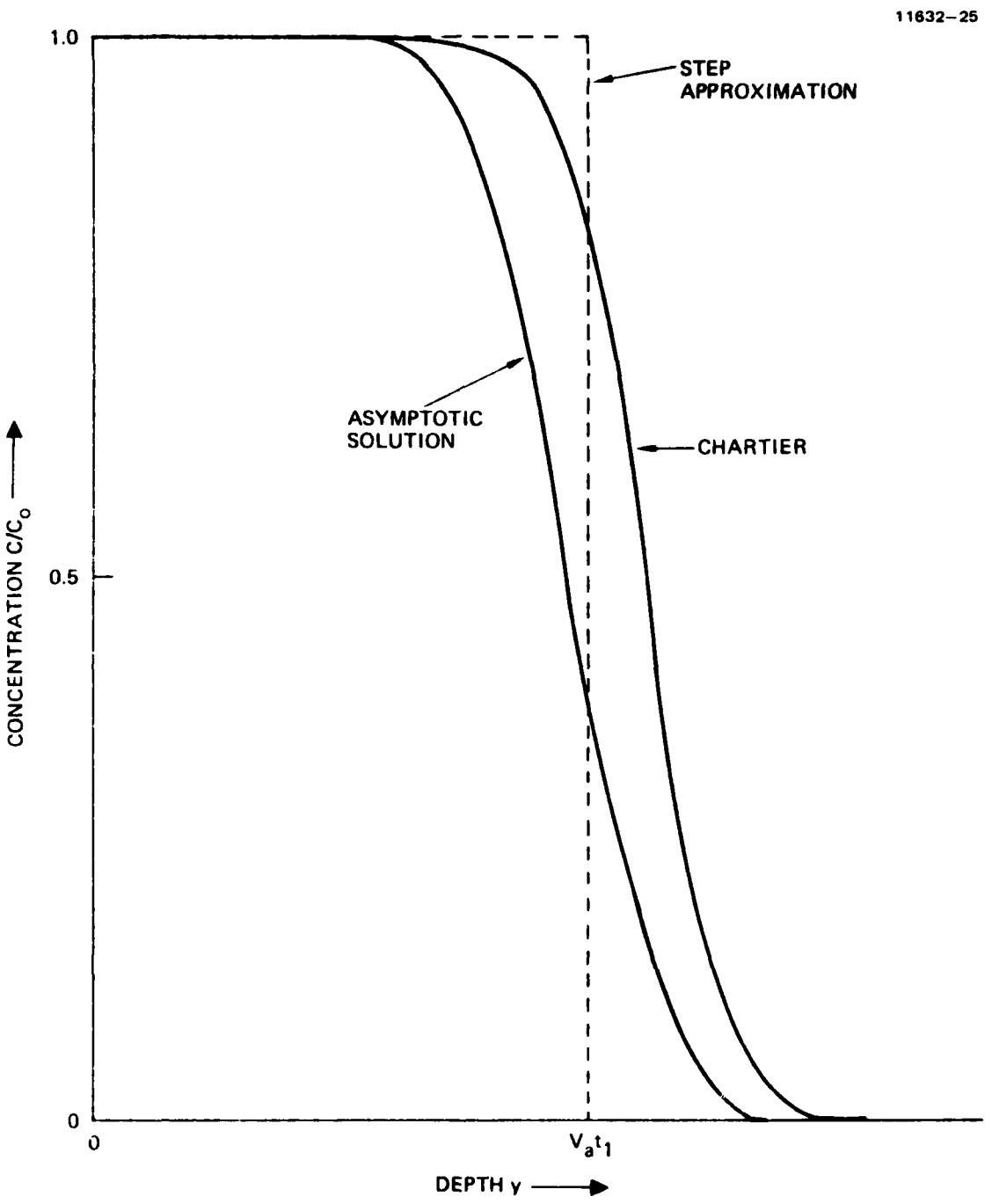

Figure 15. Theoretical Ag-profiles of ion-exchanged film waveguides. $C_n = C_o/C^n{}_n$ is the normalized source concentration, for $c_o = 0.3$.

Figure 16. Theoretical (a, b) index profiles with exchange temperature T = 616K and an exchange time t_1 = 30 min for two widths x_w of the mask window and several applied voltages, U.

These results indicate that the thinning effects observed in wide mask experiments may be controlled by varying the applied voltage, time, and mask width. Detailed measurements are therefore necessary to obtain quantitative results pertaining to a specific design of a star coupler mixing region. Clearly, the total width of region should be minimized to present mode conversion and radiation loss for the transition from channel to planar guides.

8. Refractive Index Profiling

An important aspect of further work should be the measurement of the index attained by the diffusion process. This measurement will require the development of a simple technique, one which does not require tedious and time consuming set-up procedures. It is perhaps best to utilize the refracted near-field technique, which is now operational in our laboratory, to obtain a mapping of the guide profile. The technique has been applied to profiles which lack circular symmetry; for instance, elliptical core single mode fibers by researchers at British Telecom and Plessey, Ltd., of the UK. The application of this technique is an exciting new prospect for multimode waveguide couplers.

Precise measurement of the index of refraction profile in multimode fibers is required to enable the fabrication of special profiles, such as graded index high bandwidth fibers. This technique we selected to implement is the refracted near-field method. The method is shown in Figure 17. A focused laser spot is directed on the end of the fiber. The technique uses the power escaping sideways from the core into the cladding to determine the local index of refraction. The fiber is passed through a hole in an opaque disk and is immersed in a matching oil with an index of refraction higher than the cladding index. Part of the light focused into the fiber is guided, while the rest appears outside the fiber as a hollow cone. If all of the leaky modes are blocked by the disk, the light beyond the disk varies linearly with the index of refraction at the point at which the incident light is focused. By scanning the focused spot across the fiber, the profile is obtained directly from the output of a detector that collects the light passing the disc. This method has been demonstrated at British Telecom and at Plessey, Ltd. Excellent spatial resolution has been obtained, and the capability to analyze noncircular cores has been demonstrated. In one embodiment, the precision of the index measurement was 4×10^{-5}.

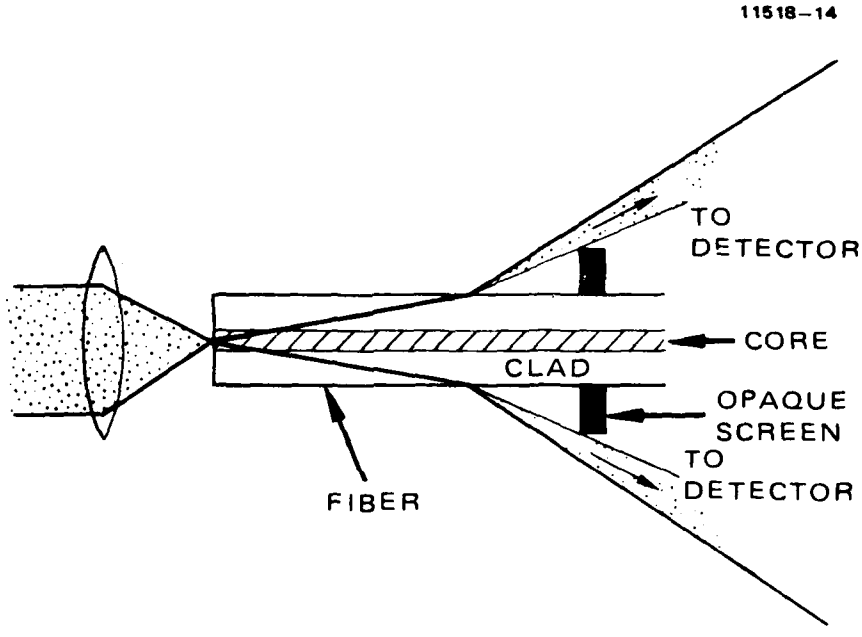

Figure 17. Refracted near-field technique for measuring the fiber index of refraction profile.

In 1981 we completed the fabrication of the index profiler and are now testing the unit. The apparatus is computer controlled and the data collection and processing is also automated. A typical profile obtained by this apparatus on a conventional fiber is shown in Figure 18. Curve 1 in this figure is a trace through the center of the core; Curve 2 is a trace through the lower half of the core; and Curve 3 is a trace through the lower quarter. Curve 1 shows the index dip that is typically found in fibers made with the internal vapor phase oxidation method.

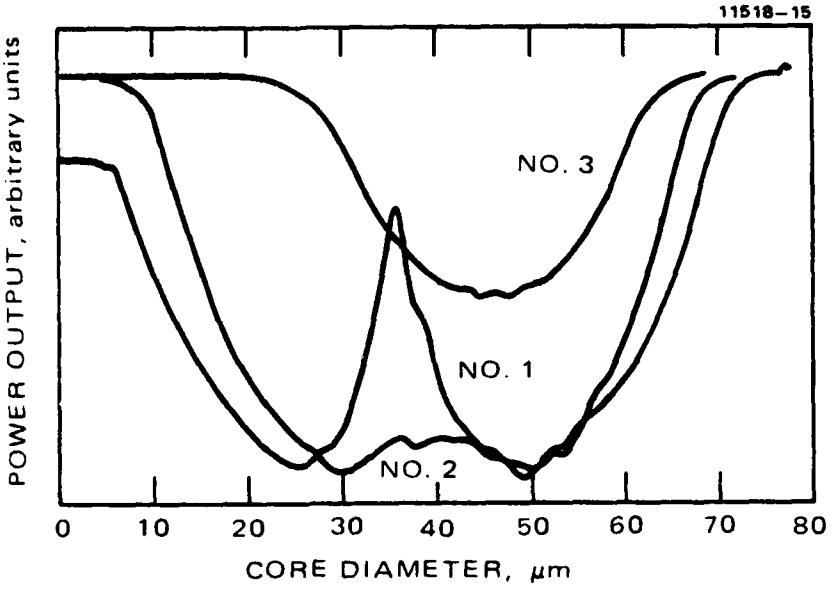

Figure 18.
Profile of a commercial fiber using the refractive near-field technique. The diffused curves pass across different sectors of the core.

B. THROUGHPUT OPTIMIZATION

1. The Optimization Process

Clearly, the most important parameter for gauging coupler performance is the maximum attainable throughput, or, equivalently, the minimum excess loss. The important technical issues for achieving high-performance couplers are the achievement of high coupling efficiency from fiber to channel to fiber (F/C/F), low waveguide absorption and scattering losses, and low internal losses due to branching. Since these issues are paramount in the minds of the ultimate users of planar couplers, our efforts during this program have emphasized throughput optimization.

Our results on throughput optimization have been taken with conventional optical fibers. Both step- and graded-index fibers have been studied. Depending on the exchange process used for guide formation, the results can be classified into three groups:

- Li_2SO_4- K_2SO_4 guides
- $AgNO_3$ field-assisted guides
- $AgnO_3/NaNO_3$ field-assisted buried guides.

To optimize throughput we have used a three-step process:

- Variation of the diffusion temperature, diffusion time, and applied field for a reasonably close first set of parameters (given set of mask openings and fiber diameter).
- Second variation of diffusion time and field for a selected group of mask openings (temperature fixed).
- Variation of the buried-gate formation parameters (temperature, time, and field) for improved throughput.

Setting the temperature to a definite value after the first trial assists in the handling of the molten salt baths and is an experimental preference. By limiting the mask width experiments to a practical range, we can lessen the number of coupling measurements that are required for the tests of structures after Step 2 (nonburied guides) or Step 3 (buried guides).

Throughput measurements were made in a straightforward manner using carefully cleaved fibers. Mode strippers were used to ensure that only guided mode coupling was being mesured. In the cases of high throughput (field-assisted Ag guides — nonburied and buried), index matching fluid was used. This is a reasonable approach since in practice index-matching epoxy will be used to attach the fibers. The fibers were manipulated on x-y-z stages to obtain maximum throughput.

2. Throughput Results on Li_2SO_4-K_2SO_4 Guides

For completeness we present previous results on Li_2SO_4 eutectic salt baths. The results of the optimization process (involving Steps 1 and 2) are summarized in Figures 19 and 20. The total throughput loss for the best case was -4.2 dB (F/C/F). By collecting all of the output light of the guide by using a lens, measurement of the fiber-to-channel coupling (F/C) and of the channel-to-fiber coupling (C/F) were obtained. Note that the fiber-to-channel (F/C) data includes the propagation loss over 1 to 2 cm of the guide.

The results for the Li_2SO_4-K_2SO_4 guides demonstrate low throughput. The index of refraction profile for these guides is not optimal in two aspects: low effective numerical aperture (NA < 0.1) is exhibited, along with a linearly

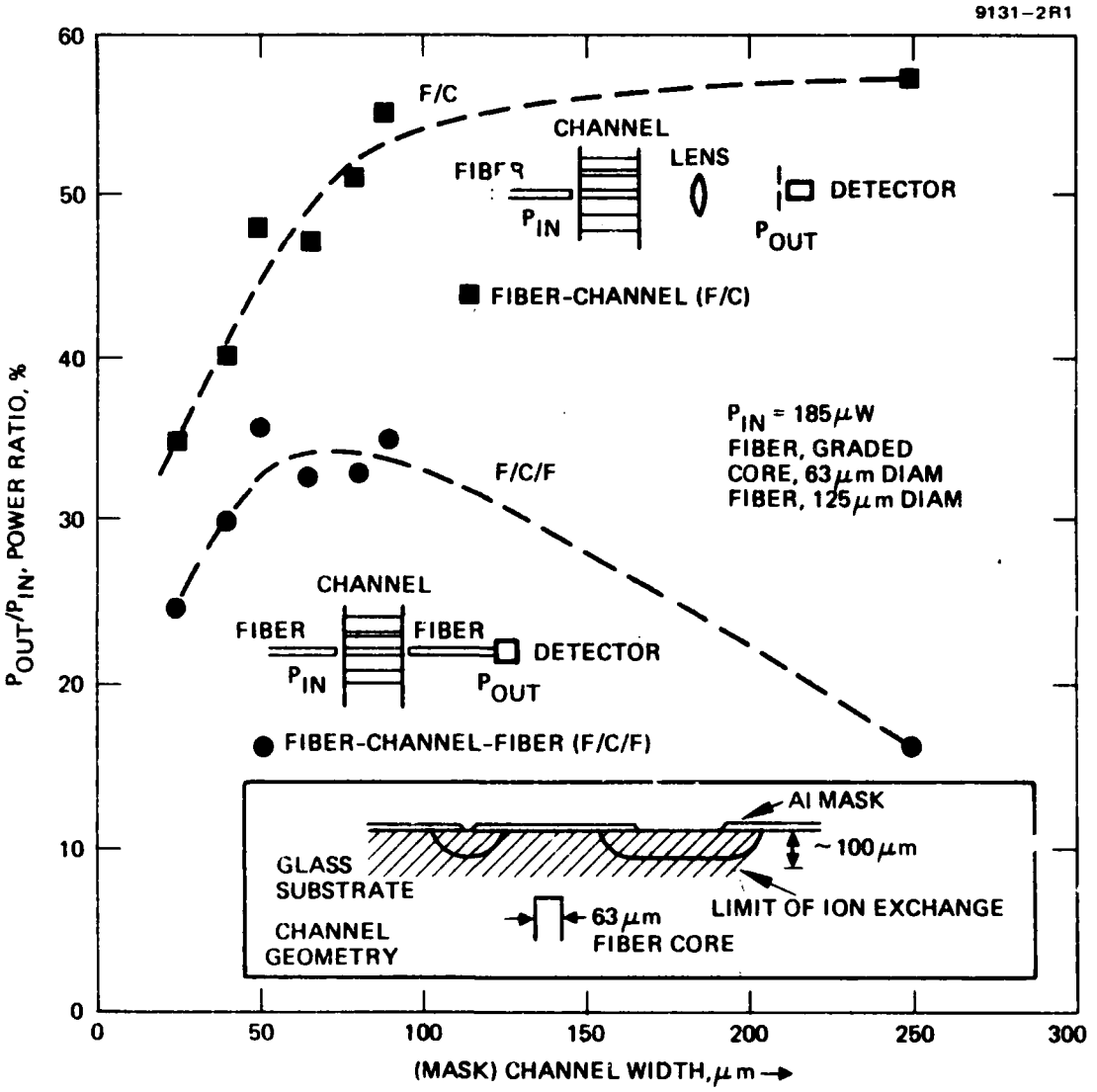

Figure 19. Power transmission ratios of constant length channels versus channel width.

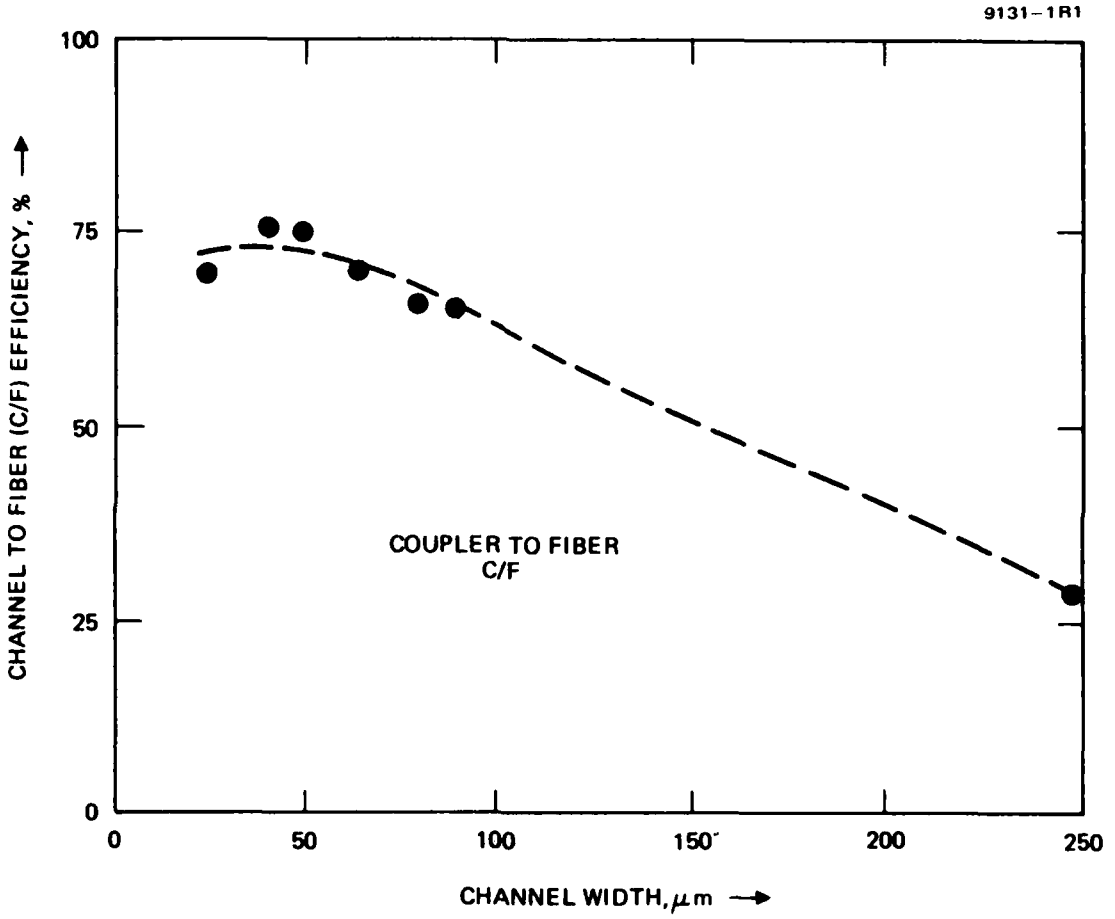

Figure 20. Channel-to-fiber coupling efficiency versus channel width.

graded index of refraction. This result suggested that a definite advantage would be gained by achieving high-index guides. Waveguide losses, while difficult to measure, are felt to be quite low (≅0.1 dB/cm) because of the very high quality of the guides. The degree of variation of the throughput results appears to be caused by surface imperfections (scratches and microcracks). For this reason, buried waveguides were considered a preferable alternative for further work.

3. Fiber-to-Channel-to-Fiber Coupling for Ag-Diffused Guides

We have concentrated on measuring the fiber-to-channel-to-fiber throughput (F/C/F) of buried channel waveguides. Optimization of the throughput is certainly the key issue facing coupler development. The results we have obtained are summarized in the following list.

- Demonstration of very high throughput (F/C/F) for buried guides with <1 dB loss and NA ≈ 0.20 input.
- Investigation of the effects of extended source excitation (such as an LED) on throughput. For an extended source, the throughput loss is <2 dB.
- Measurements of the wavelength dependence of throughput. Little wavelength dependence was found in the visible and near-infrared (to 1 μm) range.

We have measured the throughput (F/C/F) for buried waveguides using fiber excitation of NA ≈ 0.20. The results for mask widths in the range of 5 to 25 μm are independent of mask width. This result is understandably due to similar guide profiles resulting from the diffusion. It is important to recall that the Ag diffusion results in a semicircular guide of >4 times the mask width. The average value was -1.4 dB loss (F/C/F). Similar measurements were carried out on unburied waveguides. The best results obtained were -2.6 dB with the fiber NA of ≈0.18 excited. The same fiber was used for both experiments - Corning step 85 μm core (NA ≈ 0.20).

In general, meridonal ray excitation yields very low throughput loss. In fact, in our experiments we have observed <1 dB loss for selected samples. Skew ray excitation, which can be achieved in a step-index guide by moving the input spot across the input face with the input NA equal to the fiber NA, causes a degradation of the throughput. This effect has been carefully studied.

The throughput was measured as a function of the spot position on the input fiber. The NA of the excitation optics was adjusted to obtain an output NA of 0.20. The angular output scan of the fiber was measured for different spot positions on the input fiber end. A comparison of the angular scans is made for different positions in Figure 21. For each point of excitation, the throughput was carefully measured. Table 1 summarizes the results. Figure 22 presents these results in graphic form.

Table 1

Position (R)	F/C/F (dB)
0.0	-1.30
0.1	-1.40
0.2	-1.18
0.3	-1.09
0.4	-1.24
0.5	-1.40
0.6	-1.46
0.7	-1.60
0.8	-1.80
0.9	-2.00
	-1.70 dB Annular Weighted Mean

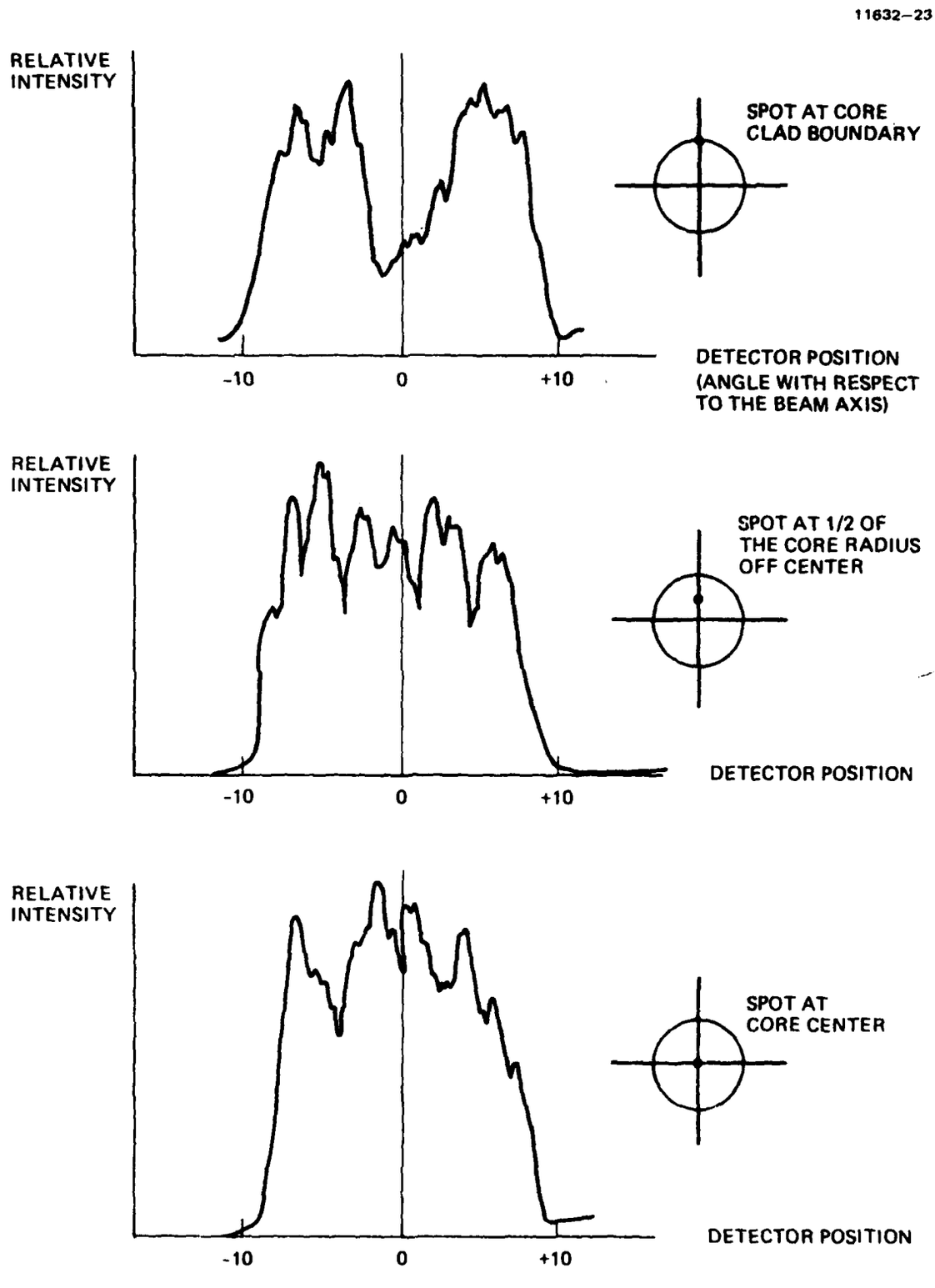

Figure 21. Intensity profile as a function of focused beam position on the diameter of a step-index fiber.

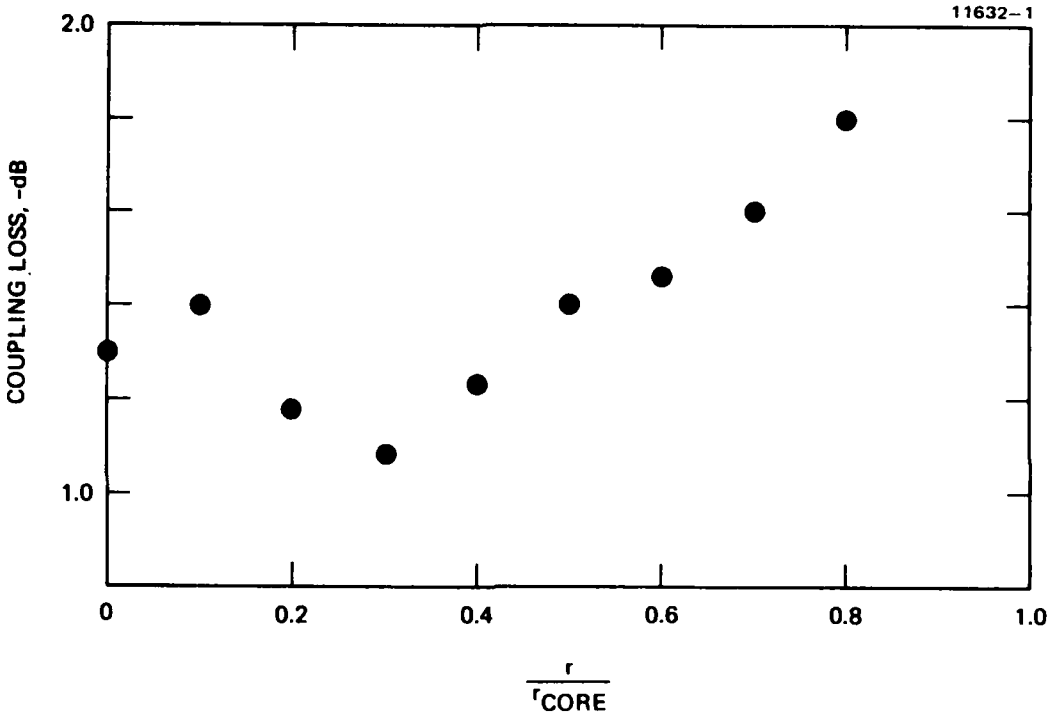

Figure 22. Fiber to channel to fiber coupling loss for different focused spot position.

The general trend is clear. The loss increases for spot positions >0.5 R. The weighted loss, taking into account the annular symmetry, is -1.7 dB. This supports the contention that an extended source excitation leads to a higher loss. We have measured the loss for a GaAs LED excitation of the fiber. The results indicate that the loss is 2.8 dB. A mandrel-wound length of fiber was used as the stripping element to ensure that leaky modes would be minimized.

The throughput loss results are now better understood because of the experiments done on variable excitation. We demonstrated that extended source excitation leads to poorer throughput results due to higher order skew mode launching. The best results obtained for meridonal ray excitation are 0.98 dB at 0.63 μm. The expected throughput for laser excitation of step-index fibers is <2 dB. Recent result indicate that this is independent of the wavelength of excitation. A spectral scan was performed of the throughput. The results are shown in Figure 23. The throughput is independent of wavelength in the visible to near-infrared range. This contrasts with the work of other researchers who use soda lime glasses.

C. CHARACTERIZATION OF BRANCH COUPLERS

We have performed detailed characterization of buried branch couplers formed by ion exchange. These experiments involve the measurement of insertion loss (or excess loss) and tapping ratio for different branch coupler angles. To enable a more comprehensive study, optical fibers with a range of core sizes (and roughly equal NAs) were used in this study.

The branch structures were formed by the double exchange process described previously. The process parameters for the guide formation are T = 300°C for $AgNO_3$, t = 7.5 min, and E = 150 V/mm. For the field-assisted burying, the parameters are T = 400°C for $NaNO_3$, t = 30 min, and E = 150 V/mm.

The output end of the 1° Y-coupler structure, when excited by a fiber input, is shown in Figure 24. The mask that we utilized is designed for 1, 2, 3, 4 and 5° angle couplers. The total length is 1.2 cm.

The insertion loss of each coupler was measured using different diameter fibers. Special step-index fibers were fabricated at HRL with 40, 57 and 101-μm cores. The fibers were excited by meridonal rays only for these measurements. The input fiber and the output fiber for the straight channel

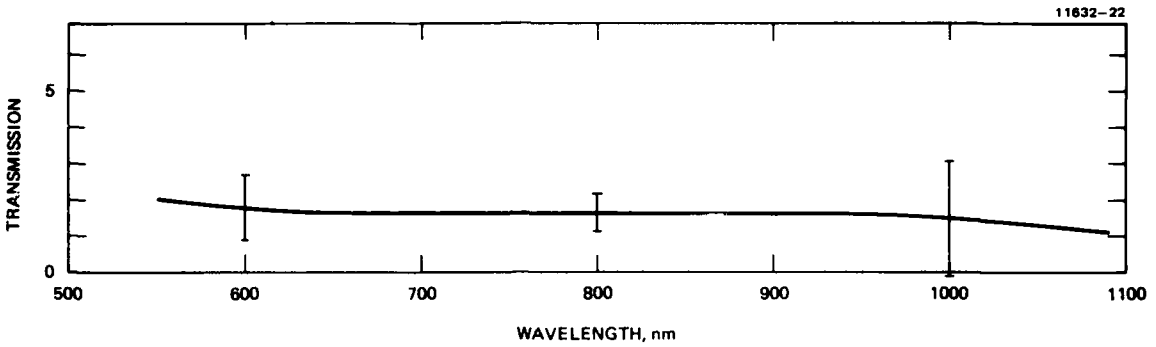

Figure 23. Spectral scan of throughput.

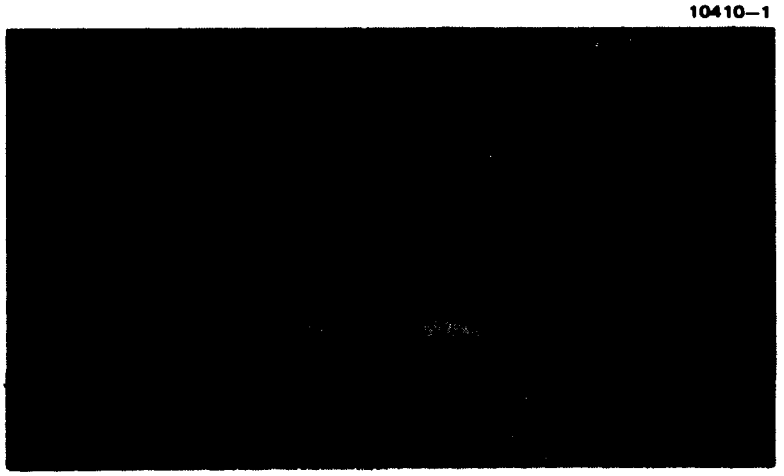

Figure 24. Planar branch couplers.

were adjusted for optimum throughput (lowest loss) of the straight channel. The output fiber for the branch was carefully moved to optimize the throughput of the branch channel with the input fiber fixed. With the fibers in position, the total throughput and tap ratio are easily measured.

The results of these measurements for a series of samples are summarized in Figures 25, 26, and 27. These figures summarize the results that are listed in Table 2. Several trends are indicated:

- The 90 μm core fiber produces the best insertion loss results.
- The insertion loss is in the 2- to 3-dB range, dominated by sample imperfections which are mainly edge imperfections.
- The variance in the tap ratio is large (±1 dB) if the approach of optimizing throughput is taken.

We extended the branch coupler characterization by varying the input fiber launching condition. We excited both meridonal and skew rays in the input fiber to investigate the effect of fiber excitation conditions on the coupler insertion loss and tapping ratio.

The sample used in the measurement contains five asymmetric Y-coupler structures with 1, 2, 3, 4, and 5-degree branching angles, respectively. These structures were formed by the field-assisted double ion-exchange process in a glass substrate. The waveguide cross-sectional geometry is roughly an ellipse, with major and minor axes of 100 μm and 45 μm, respectively.

Corning step-index fibers with 85-μm core diameters were used at both input and output ends of the couplers. The input fiber is excited by focusing a He-Ne laser on the end face of the fiber, as shown in Figure 28. The focused laser spot position is varied from position 0 to 3 during the experiment. Meridonal ray excitation corresponds to input spot at position 0, and skew rays are excited when the input spot is at positions 1, 2, and 3.

The measured results of the coupler total insertion loss and branching ratios are summarized in Table 3 and plotted in Figures 29, 30, and 31. It is interesting to note that the insertion loss and tapping ratios vary monotonically as the laser spot is moved from position 1 to 3. However, for position 0 excitation, the total insertion loss is higher than that obtained when the input spot is at 1. We believe that the index dip at the fiber core center acts as a scatterer and excites lossy higher order modes in the waveguide. As

Table 2. Branch Angle

11632-2

	1°	2°	3°	4°	5°	CORE	N.A.
TR NO. 1	-3.0	-1.9	-1.6	-0.6	-0.3	40 μm	0.22
TR NO. 2	-3.0	-4.4	-5.1	-8.7	-11.2		
TIL	-3.3	-2.7	-4.0	-3.5	-3.1		
TR NO. 1	-1.7	-2.4	-1.8	-1.2	-0.7	57 μm	0.20
TR NO. 2	-4.9	-3.7	-4.8	-6.3	-8.2		
TIL	-3.5	-2.6	-3.3	-3.4	-3.1		
TR NO. 1	-2.4	-2.6	-2.0	-1.4	-0.9	90 μm	0.18
TR NO. 2 (A)	-3.7	-3.5	-4.3	-5.7	-7.2		
TIL	-3.0	-2.3	-2.5	-2.4	-2.2		
TR NO. 1	-2.7	-2.8	-2.0	-1.4	-1.0		
TR NO. 2 (B)	-3.3	-3.2	-4.3	-5.6	-6.7		
TIL	-2.1	-2.8	-2.4	-2.5	-2.9		
TR NO. 1	-2.2	-1.9	-1.5	-1.0	-0.6	100 μm	0.18
TR NO. 2	-4.1	-4.5	-5.2	-6.7	-8.6		
TIL	-3.4	-2.7	-3.2	-3.1	-3.2		

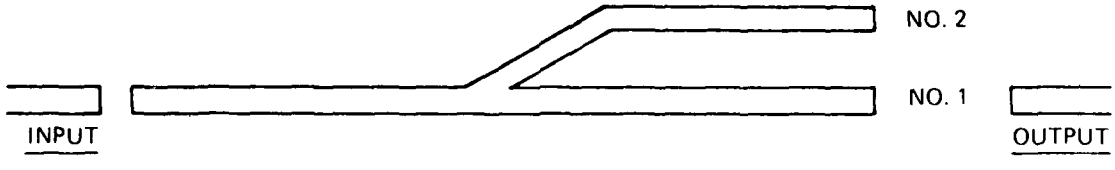

TR TAP RATIO
TIL - TOTAL INSERTION LOSS
SAMPLES A AND B ARE SETS OF COUPLERS FROM THE SAME SUBSTRATE

Table 3. Data Summary

Input Fiber Excitation Position			Coupler Branch Angle				
			1°	2°	3°	4°	5°
0	Tap Ratio	A	-2.6	-2.4	-2.1	-1.5	-1.1
		B	-3.5	-3.7	-4.2	-5.3	-6.5
	Insertion Loss		2.7	3.2	3.0	2.6	3.3
1	Tap Ratio	A	-2.5	-1.8	-1.5	-1.2	-0.7
		B	-3.6	-4.7	-5.5	-6.3	-8.5
	Insertion Loss		2.3	2.5	2.4	2.3	2.8
2	Tap Ratio	A	-2.8	-2.3	-2.2	-1.4	-1.0
		B	-3.2	-3.9	-4.0	-5.6	-7.0
	Insertion Loss		3.2	3.4	3.5	3.4	3.8
3	Tap Ratio	A	-3.1	-2.7	-2.3	-1.9	-1.5
		B	-2.9	-3.3	-3.9	-4.6	-5.5
	Insertion Loss		4.1	4.4	4.4	4.3	5.0

NOTE: (All numbers are in dB)

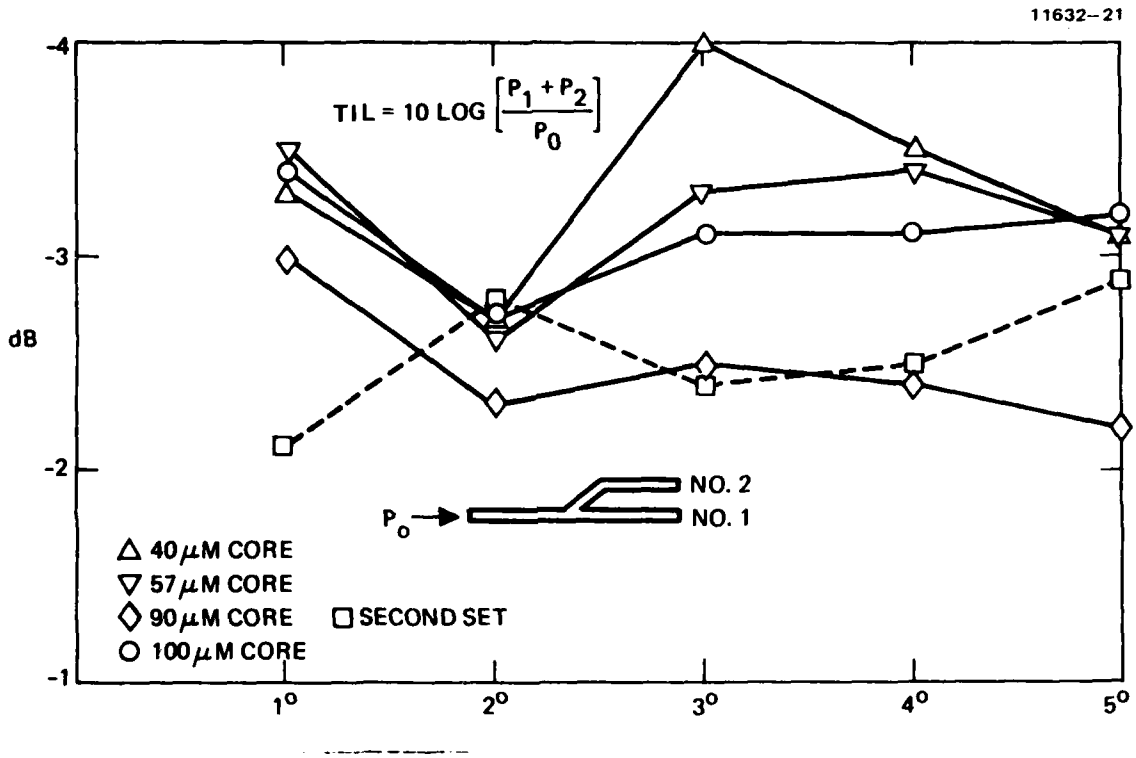

Figure 25. Total insertion loss (T.I.L.) as a function of coupler angle. Four (4) fiber core sizes.

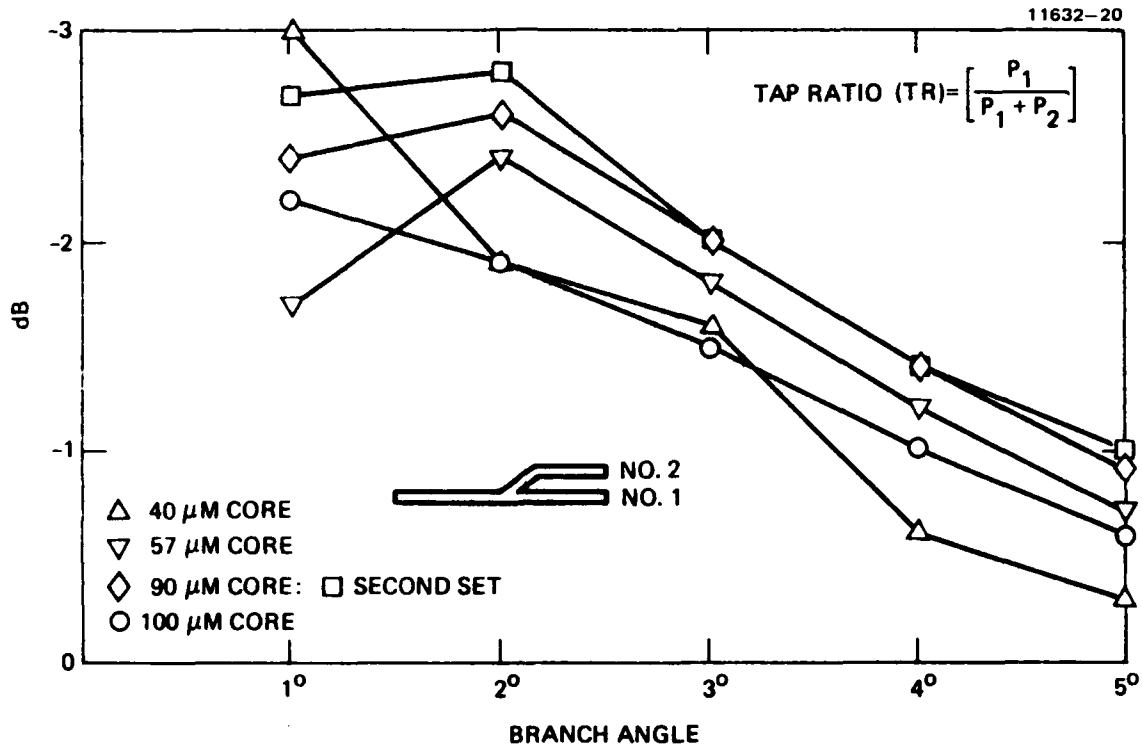

Figure 26. Tap ratio for Branch No. 1 as a function of coupler angle. Four (4) fiber core sizes.

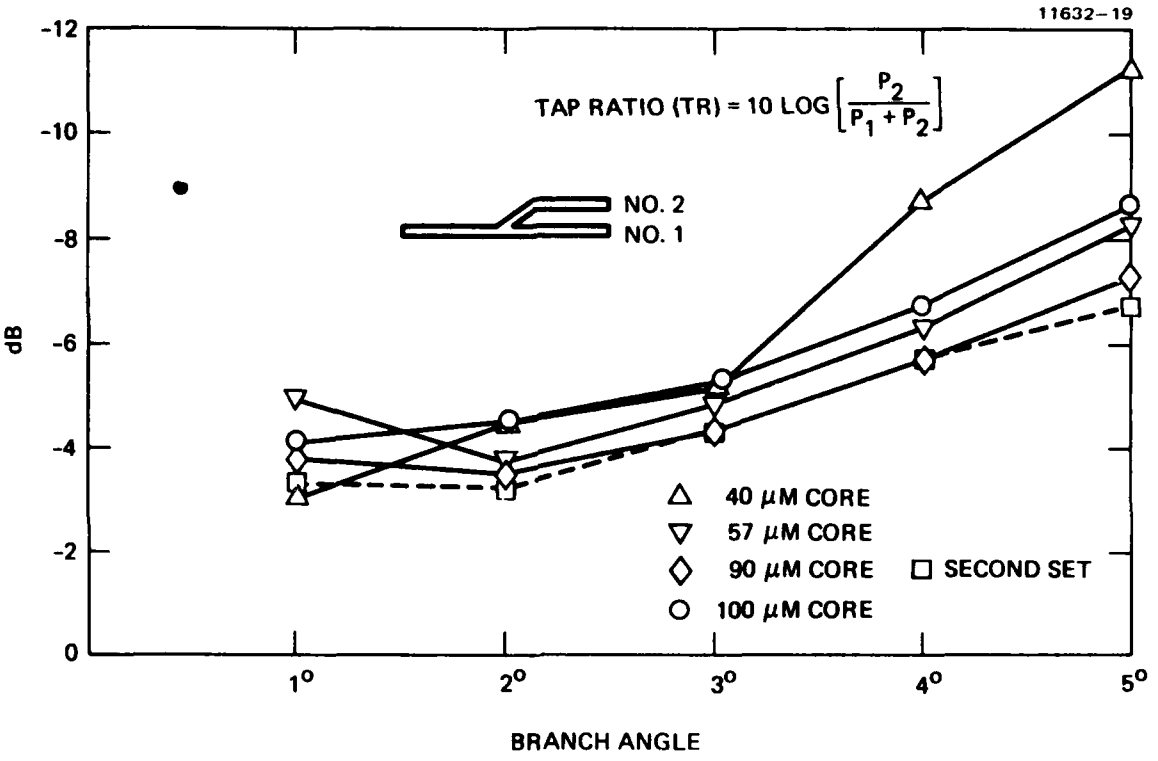

Figure 27. Tap ratio for Branch No. 2 as a function of coupler angle. Four (4) fiber core sizes.

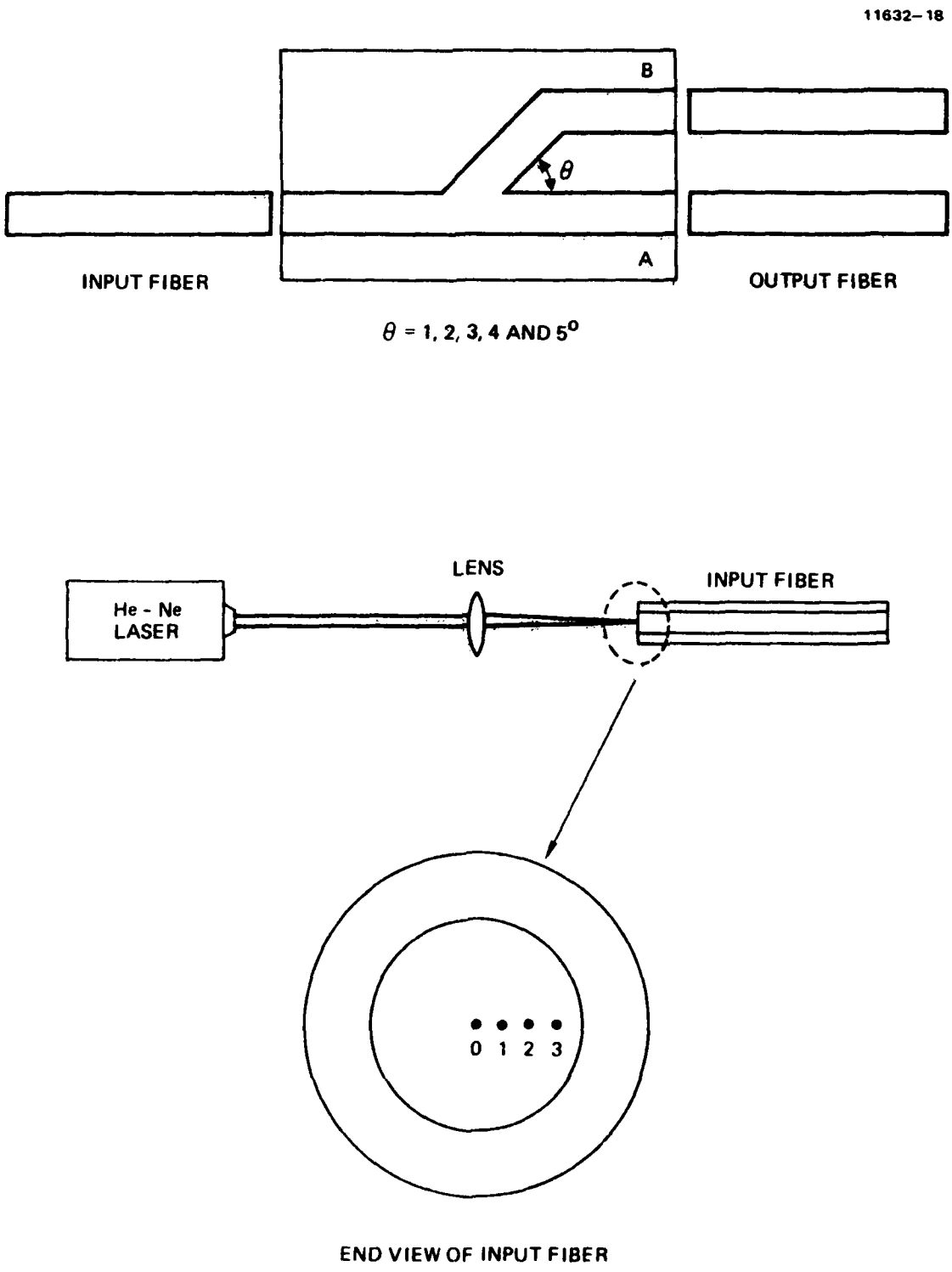

Figure 28. Experimental setup and fiber excitation arrangement.

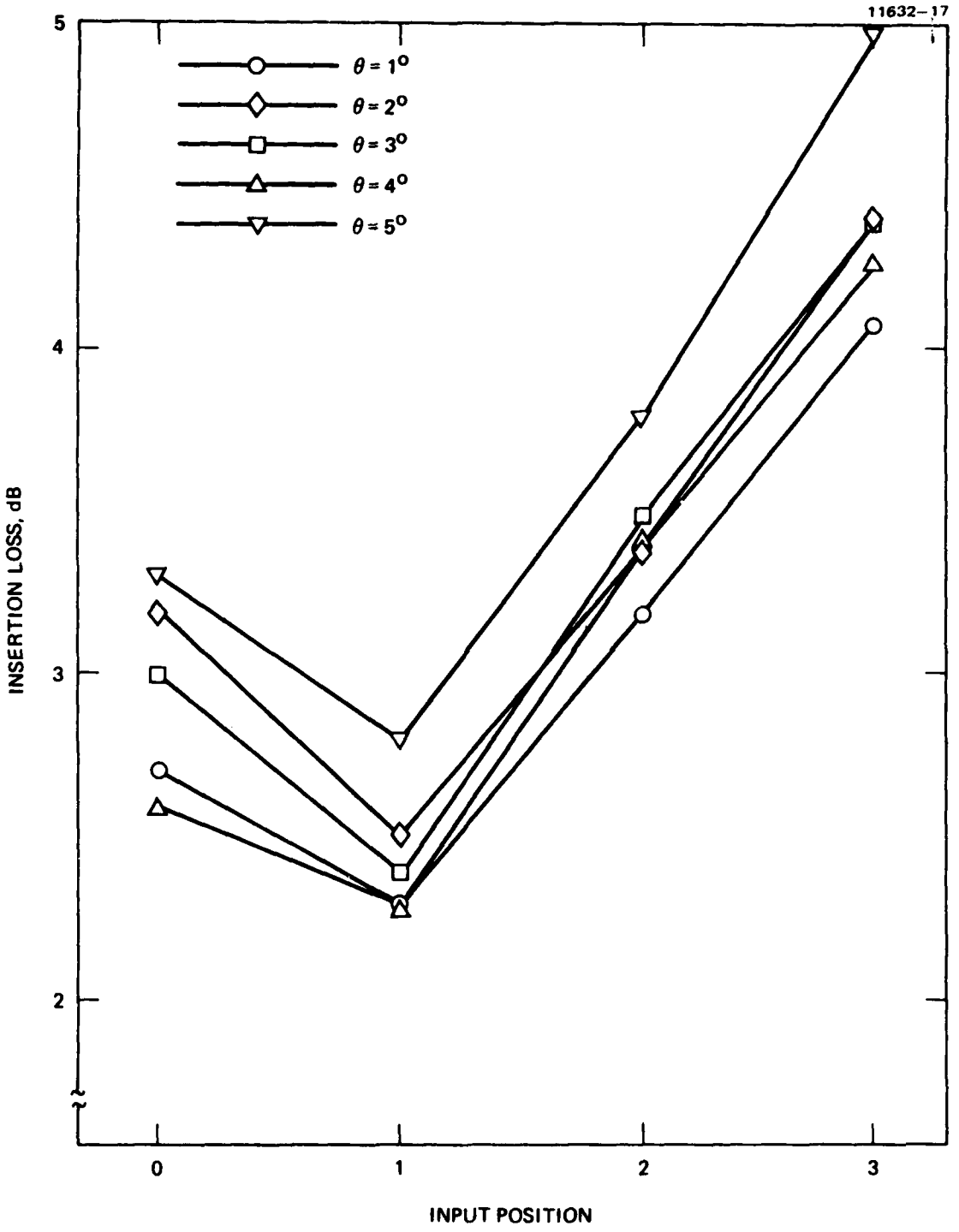

Figure 29. Coupler insertion loss as a function of input fiber excitation condition.

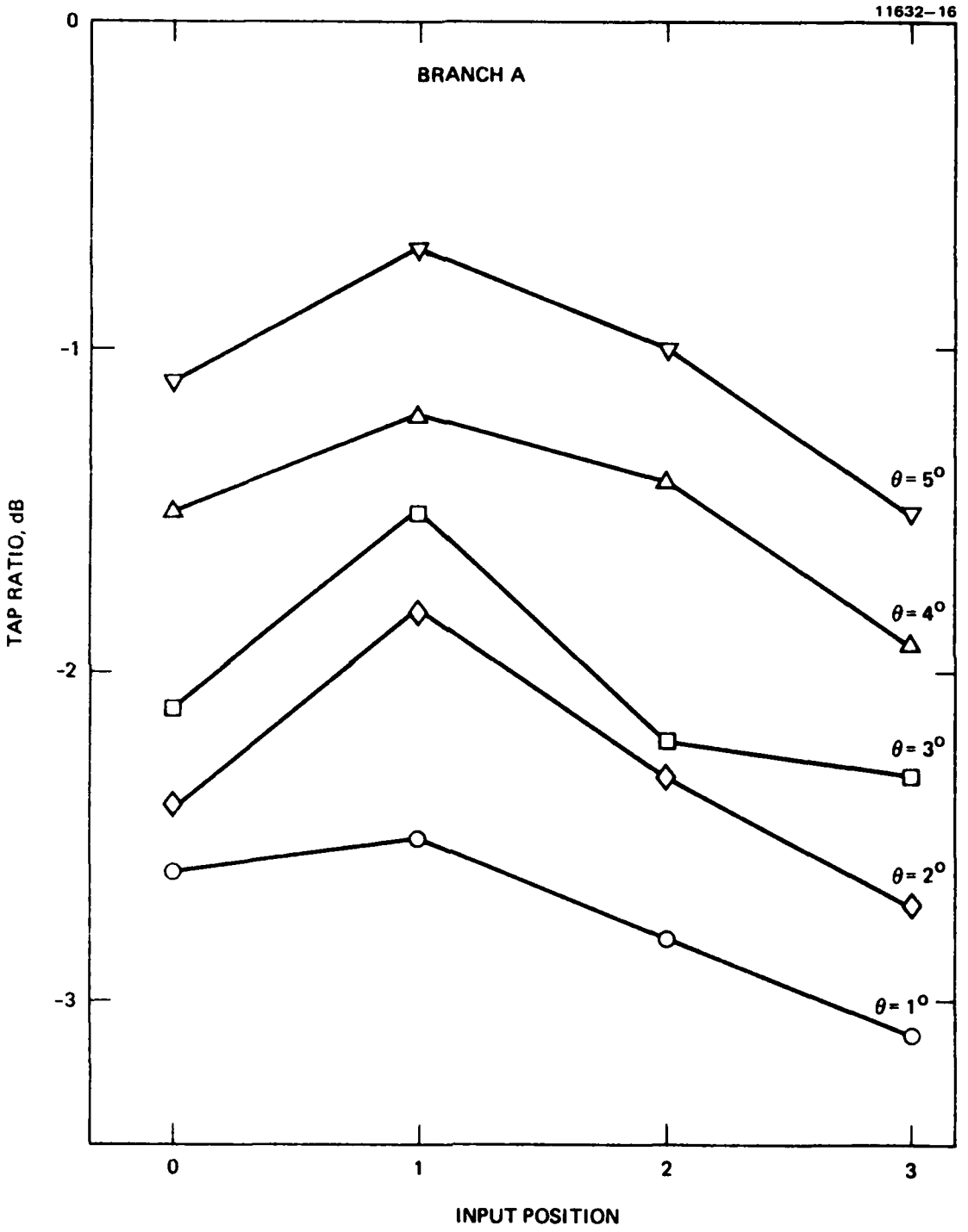

Figure 30. Branch A tap ratio versus fiber excitation condition.

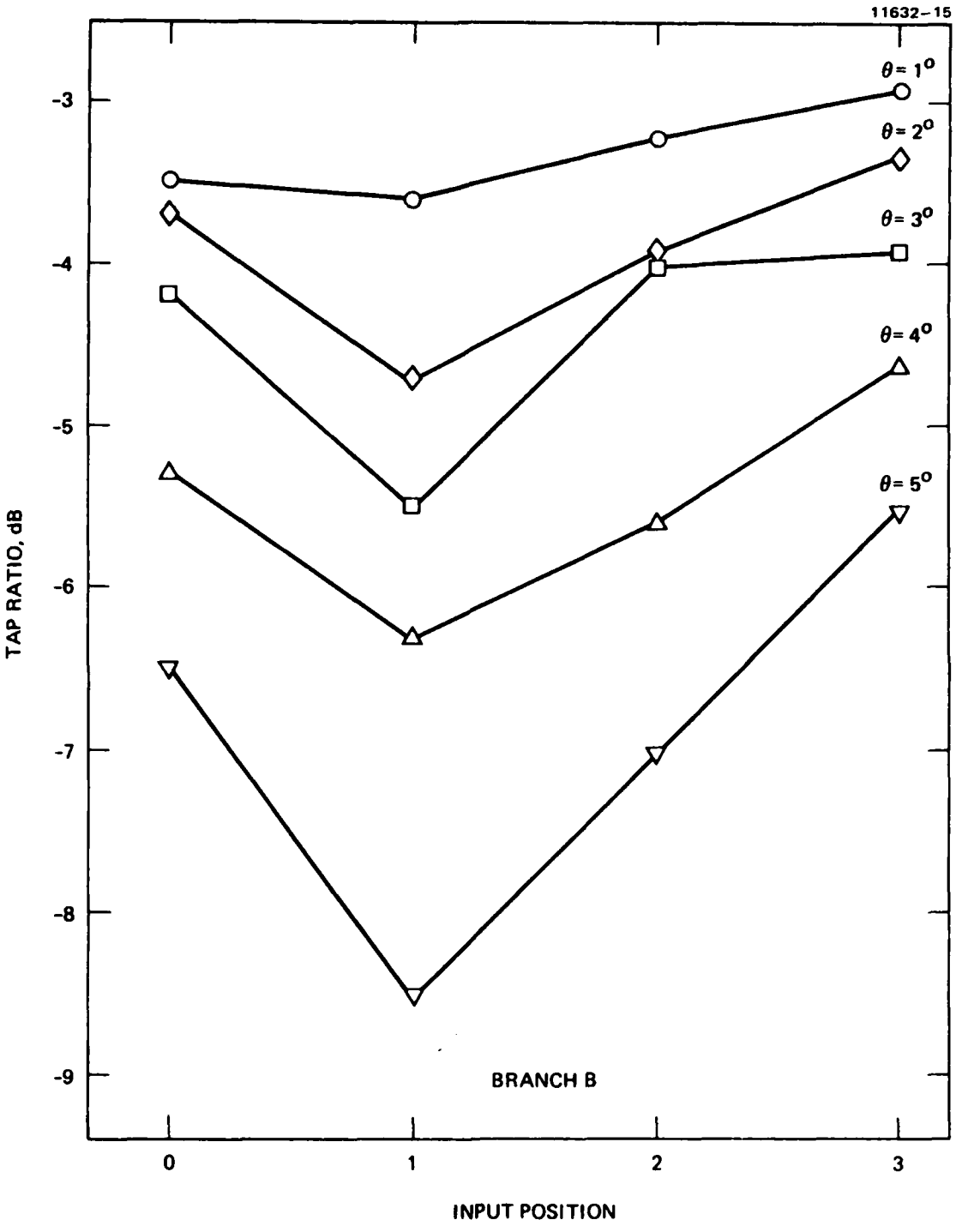

Figure 31. Branch B tap ratio versus fiber excitation conditions.

a result, the coupler performance appears inferior for on-axis excitation. Improvements in these measurements can certainly be made in optical fibers made by outside process (OVP) or vapor axial deposition (VAD). These fibers have no index hole at the center, due to GeO_2 evaporation.

D. THEORETICAL MODELING OF THE COUPLING PROCESS

We carried out calculations to determine the optimal conditions for coupling optical power in and out of an ion-exchanged glass-channel-waveguide using multimode fibers. A schematic of the coupling geometry is shown in Figure 32.

To simplify the calculation, we assume that the waveguide cross section is of simple geometrical shape, such as a semicircle or an ellipse. Furthermore, the optical power distribution is assumed to be uniform across the entire area of the fiber core and the guide. The optimum coupling condition is reached when the geometrical overlap between the fiber core region and the waveguide cross section is the largest.

In the calculation the waveguide size is fixed, while the fiber core diameter and the fiber location are variable. The geometrical overlap between the fiber core and the waveguide is evaluated and designated as H. In accord with the representation in Figure 33, the coupling coefficient from the input fiber to the channel guide is given by

$$T_1 = H/A_F \quad , \tag{17}$$

where A_F is the fiber core area. Likewise, at the output end the coupling efficiency of optical power from waveguide back into the fiber is

$$T_2 = H/A_W \quad , \tag{18}$$

where A_W is the waveguide cross-sectional area. Thus, the total throughput for fiber-to-waveguide-to-fiber transmission is given by

$$T = T_1 \, T_2 = H^2/A_F \, A_W \quad . \tag{19}$$

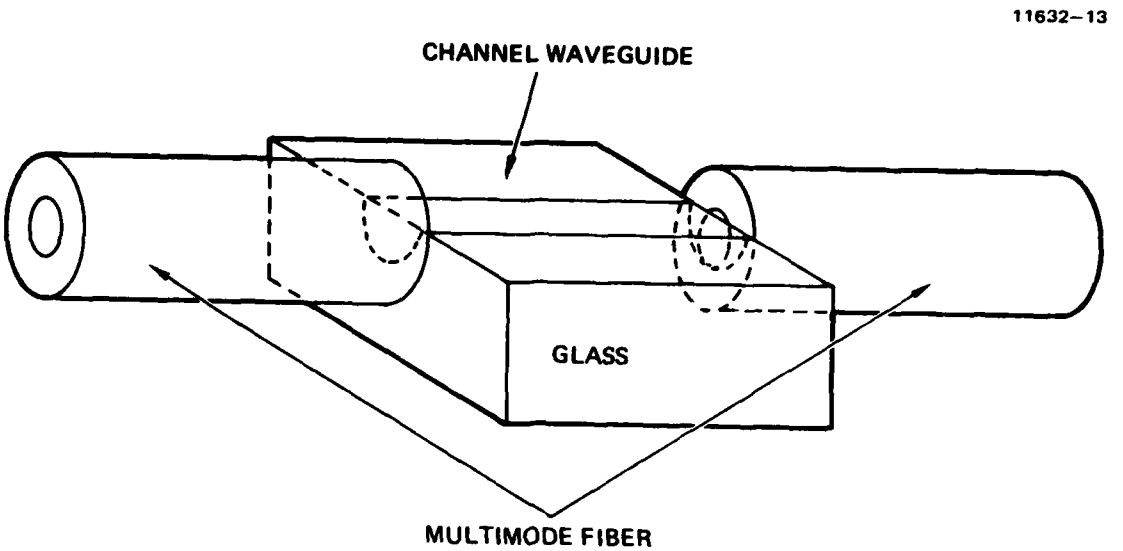

Figure 32. Geometry of fiber-to-waveguide-to-fiber coupling.

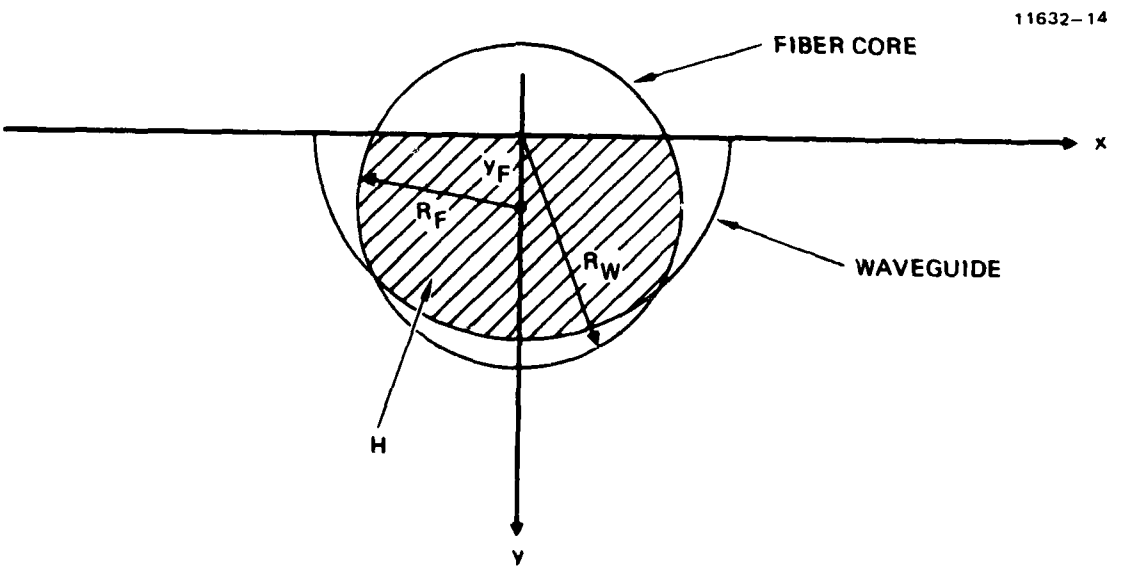

Figure 33. Calculation of the geometrical overlap, H, with a semi-circular waveguide cross section.

We will first consider the case where the waveguide has a semicircular cross section. The waveguide can be described mathematically as the region enclosed by the straight line, $y = 0$ (X-axis), and the curve, $X^2 + y^2 = R_W^2$, because $y > 0$, where R_W is the radius of the semicircle. Similarly, the fiber core boundary is described by the circle,

$$X^2 + (y - y_F)^2 = R_F^2 \quad , \tag{20}$$

where R_F is the fiber core radius, and y_F is the fiber axis location. The overlapping region, H, is indicated in Figure 34 by the cross-hatched area. If we normalize all the lengths to R_W, so that $R_F/R_W = R$, then $y_F/R_W = y_o$, and H can be shown to be

$$\begin{aligned} H = \pi/2 - P(1 - P)^{1/2} - \sin^{-1} P + (P - y_o)(R^2 - y_o^2 + 2y_o P - P^2)^{1/2} \\ + R^2 \sin^{-1} |(P - y_o)/R| + y_o (R^2 - y_o^2)^{1/2} + R^2 \sin^{-1} (y_o/R) \quad , \end{aligned} \tag{21}$$

where $P = (1 - R^2 + y_o^2)/2y_o$. In a normalized unit the cross-sectional area of the waveguide is $A_W = \pi/2$, and that of the fiber is $A_F = \pi R^2$. Using Equation (19) we can find the total throughput,

$$T = 2(H/\pi R)^2 \quad . \tag{22}$$

Figure 34 is a plot of total insertion loss, T, as a function of the fiber axis position, y_o, with the fiber core radius, R, as a parameter. The minimum insertion loss (-2.1 dB) occurs when $R \approx 0.7$ and $y_o \approx 0.42$. Although this model is over-simplified, good qualitative and quantitative agreement with experimental results are obtained. Also note that we have neglected the reflection and propagation losses in this calculation.

For buried glass channel guides, the cross section sometimes is better described by an ellipse. The coupling geometry is shown in Figure 35. The fiber core boundary is prescribed by the equation,

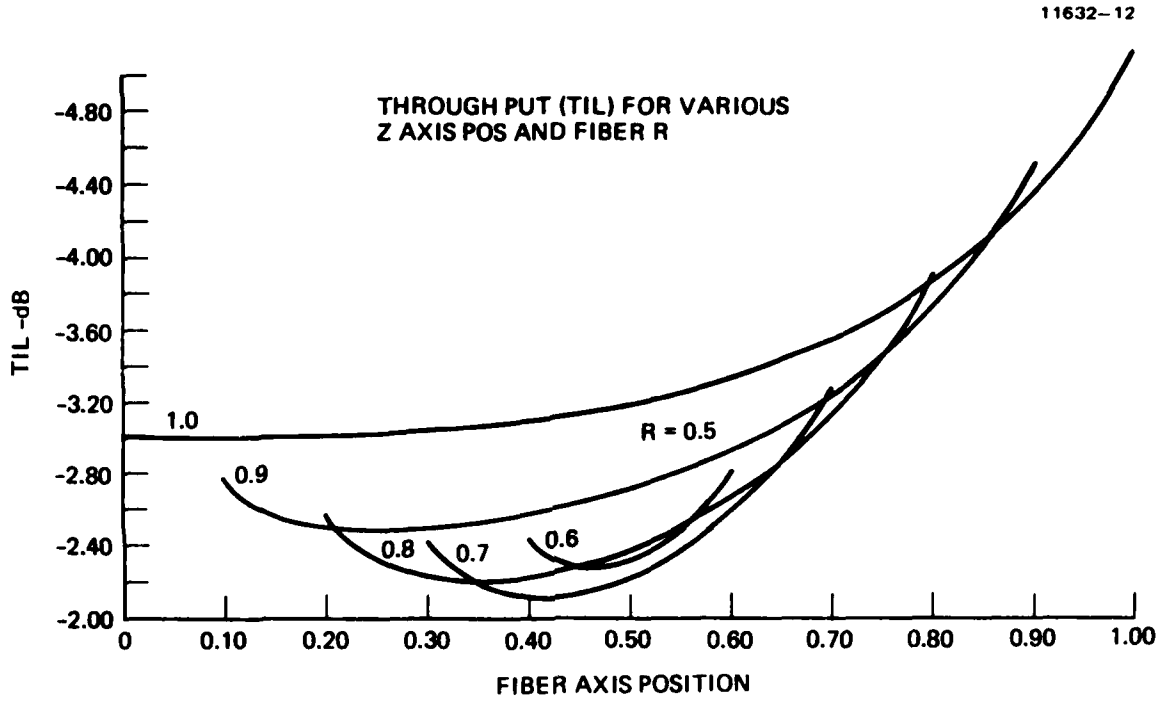

Figure 34. Insertion loss for fiber-to-semi-circular waveguide-to-fiber coupling with fiber core radius as a parameter.

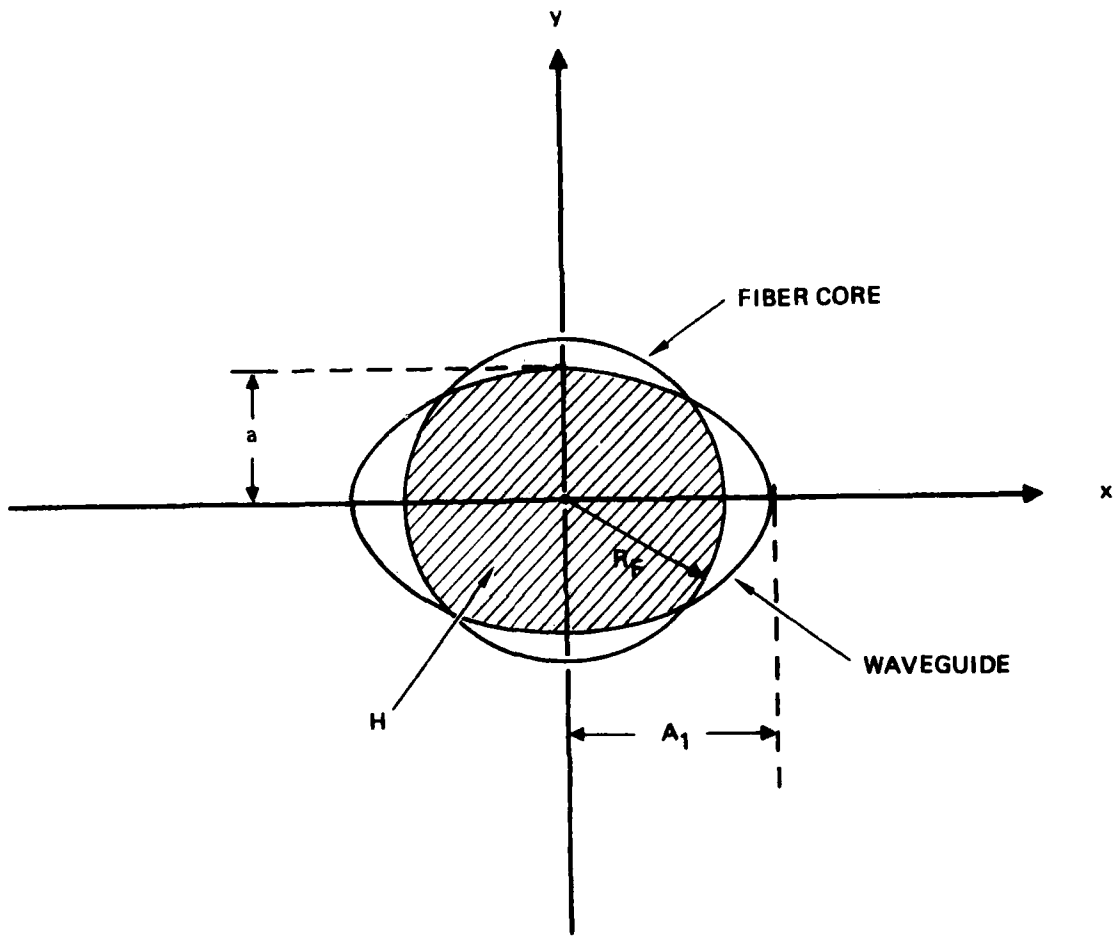

Figure 35. Coupling between fiber and channel guide with elliptical cross section.

$$X^2 + y^2 = R_F^2 \quad , \tag{23}$$

and the waveguide is enclosed by the curve

$$X^2/A_1^2 + y^2/a^2 = 1. \tag{24}$$

The overlap region, H, is given by

$$H = 2\pi - 2AP\,(1 - P^2)^{1/2} - 2A \sin^{-1} P + 2P(R^2 - P^2)^{1/2} + 2R^2 \sin^{-1} (P/R) \quad , \tag{25}$$

where $P = [(A^2 - R^2)/(A^2 - 1)]^{1/2}$ for $1 \leq R \leq A$, and all of the lengths are normalized to a, the minor axis of the ellipse, so that $R_F/a = R$ and $A_1/a = A$. The total insertion loss in this case is

$$T = H^2/A_W A_F = (H/\pi R)^2/A \quad , \tag{26}$$

which is a function of the fiber core radius, R, and the waveguide ellipticity, A.

In Figure 36 the insertion loss, T, is plotted as a function of R, with A as a parameter. The increment of A in the graph is 0.1. Note that A = 1 represents a circular waveguide; therefore A = 1 and R = 1 should correspond to the perfect overlapping condition. The family of curves in Figure 36 shows that there is a best value of R for a given waveguide ellipticity. This result has been verified experimentally with selected values of R and A.

E. COUPLER PACKAGING AND FIBER INTERFACING

The packaging of a 3-dB power divider was successfully accomplished. It consists of a planar asymmetrical Y-coupler with three pigtailed multimode fibers enclosed in a metallic box. The alignment process is as follows. A piece of multimode fiber was aligned to the input port of the Y-coupler and a second fiber was aligned to the straight-through port. The two fibers

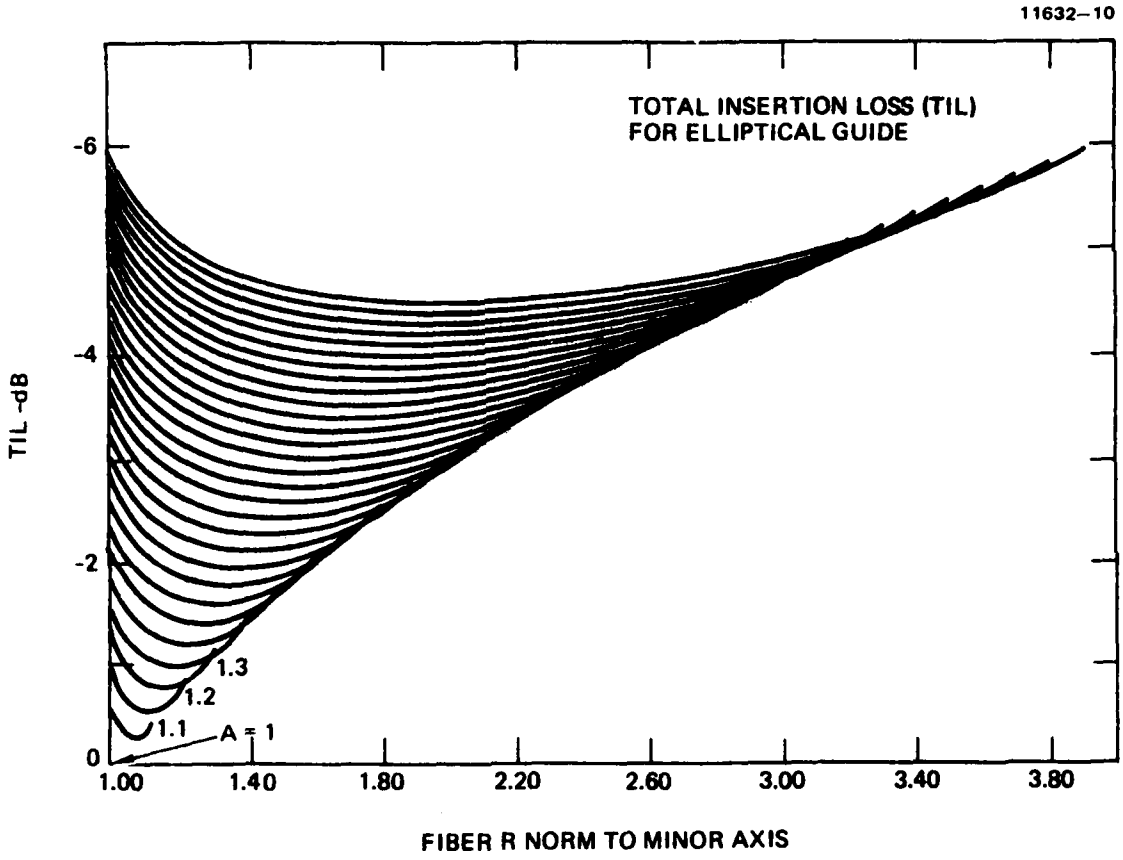

Figure 36. Insertion loss for fiber-to-elliptixal guide-to-fiber coupling with waveguide ellipticity as a parameter.

were positioned so that the straight-through signal was optimized. The input fiber was then permanently attached to the planar structure with epoxy. This was followed by attachment of the second fiber to the straight through output port, also with epoxy. Finally, a third fiber was aligned to the remaining output port to complete the device. The alignments were carried out with the aid of X-Y-Z micro- positioners under a stereoscope. After the fibers were fixed in place, a piece of glass (roughly 1 cm x 1.6 cm x 0.3 cm) was epoxied on top of the waveguide to serve as a protection for the waveguide and to provide mechanical support for the fibers. Figure 37 shows one such finished device. The measured total insertion loss of the power divider is approximately 2 dB. The power ratio of the two outputs is nearly unity. Figure 38 shows a packaged power divider in operation. One such device will be delivered to RADC at the end of the contract.

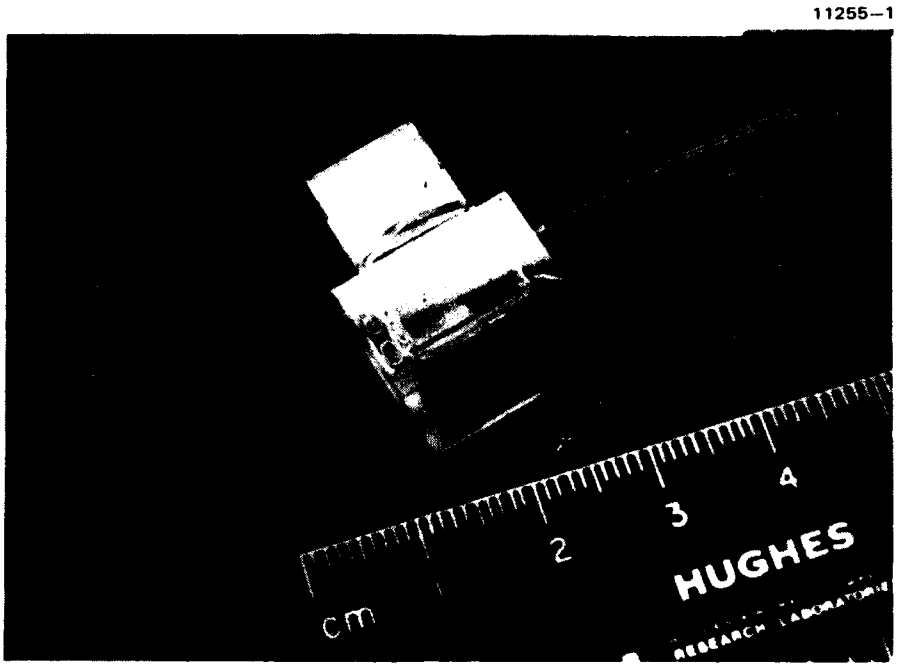

Figure 37. A fiber pigtailed planar Y-coupler.

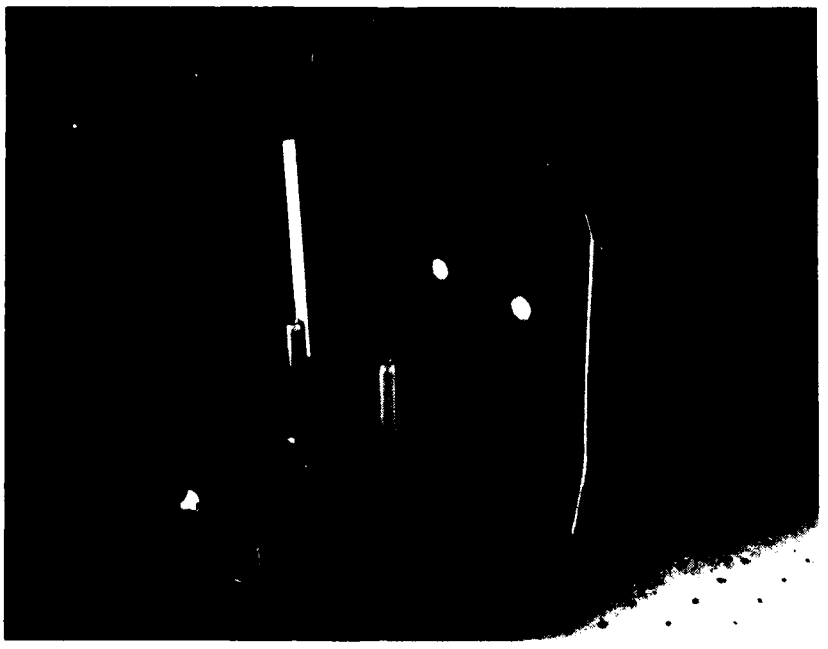

Figure 38. A packaged 3-dB Y-coupler with the two fiber outputs displayed on a screen.

REFERENCES

1. G.L. Tangonan, L.E. Gorre, and D.L. Persechini, Optics Comm. 27, 358 (1978).

2. F. Auracher, H. Boroffa, and R.Th. Kersen, Technical Digest of the Integrated Optics Conference, January 12-14, 1976, Salt Lake City, Utah, Paper MD-1.

3. M.G.F. Wilson, C.W. Pitt, R. Manku, A.O. de Oliviera, and O. Parriaux, Electron. Lett. 12, 434 (1970).

4. G.L. Tangonan, O.G. Ramer, L.E. Gorre, H.R. Friedrich, C.K. Asawa, M.K. Barnoski, and D.L. Persechini, Topical Meeting on Optical Fiber Communications, March 6-8, 1979, Washington, D.C., Paper WC2

5. G.L. Tangonan, O.G. Ramer, H.R. Friedrich, C.K. Asawa, D.L. Persechini, and L.E. Gorre, Technical Digest of the Optical Communications Conference, Amsterdam, The Netherlands, September 17-19, 1979, Paper 21.5.

6. G.H. Chartier, P. Jassaud, A.D. de Oliviera, and O. Parriaus, Electron. Lett. 13, 763 (1979).

7. G.H. Chartier, P. Jassaud, A.D. de Oliviera, and O. Parriaux, Electron. Lett. 14, 132 (1978).

8. T. Izawa and H. NaKagome, Appl. Phys. Lett. 21, 584 (1972).

9. G.L. Tangonan, D.L. Persechini, and C.K. Asawa, Advance in Ceramics, Vol. 2, Physics of Fiber Optics, 463 (1981).

10. E. Aksenov, A.A. Lipovskii, A.J. Paulenko and G. Yu Sotnikova, Soviet Phys - Tech. Phys. 2614, 524 (1981).

11. G. Chartier, P. Collin, A. Guez, P. Jaussand, and Y. Von, Appl. Opt. 19, 1092 (1980).

12. E. Voges, Proceedings of the Int. School of Quantum Electronics, Erice, Sicily, August 17-29, 1981; preprint given to G.L. Tangonan of HRL.

13. A.E. Cooper and M. Abouel-Leil, Appl. Opt. 19, 1091 (1980)

14. D.E. Day, Amorphous Materials (Wiley, New York, 1972).

15. K.S. Spiegler and C.D. Cryell, J. Phys. Chem. 56, 106 (1952).

16. M. Abouel-Leil, Ph.D. Thesis, Case Western Reserve University, Cleveland, Ohio (1978).

17. H. Ohta and M. Hara, Rep. Res. Lab. Asahi Glass 20(1),14 (1970).

18. G.H. Chartier, Electronic Lett. 14, 132 (1978).

19. O.G. Ramer, Appl. Opt. 19,1294 (1980).

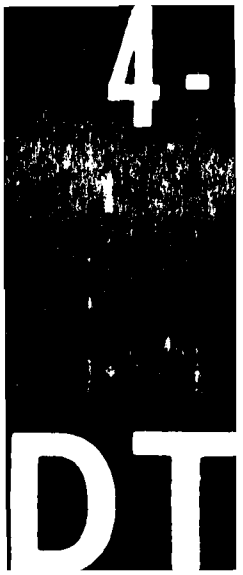
4-
DT